entropy

MDPI

Article

Enhancing s-CO_2 Brayton Power Cycle Efficiency in Cold Ambient Conditions Through Working Fluid Blends

Paul Tafur-Escanta [1], Luis Coco-Enríquez [2,*], Robert Valencia-Chapi [1] and Javier Muñoz-Antón [3]

[1] Universidad Técnica del Norte, Ibarra 100150, Ecuador; rmvalencia@utn.edu.ec (R.V.-C.); pmtafur@utn.edu.ec (P.T.-E.)
[2] Luxoft (DXC Technology), Madrid 28232, España.
[3] Universidad Politécnica de Madrid, Madrid 28006, España; jamunoz@etsii.upm.es (J.M.-A.)
* Correspondence: luiscocoenriquez@hotmail.com (L.C.-E.)

Abstract: Supercritical carbon dioxide (s-CO_2) Brayton cycles have been identified as a potentially effective solution for high-efficiency energy conversion, primarily due to their compact design and favorable thermophysical properties. Nevertheless, performance limitations have been observed in cold environments, including those in Greenland, Russia, Canada, Sweden, Norway, Finland, Alaska, and other regions. The present study has been developed since an investigation into the recompression Brayton cycle (RBC), specifically the performance benefits of blending CO_2 with low-critical-temperature additives (Methane (CH_4), Tetrafluoromethane (CF_4), Nitrogen Trifluoride (NF_3) and Krypton (Kr)) to form alternative working fluids that are better suited to sub-zero conditions. The findings of this study demonstrate that the implementation of CO_2-CH_4 and CO_2-CF_4 rich mixtures has the potential to enhance thermal efficiency by up to 10 percent absolutely when compared with pure CO_2 cycles. Furthermore, it was demonstrated that CO_2-NF_3 mixtures exhibited notable efficacy at moderate sub-zero conditions, while CO_2-Kr mixtures exhibited modest yet consistent improvements. The simulation results confirmed that, in high-efficiency configurations, HTR became the limiting component, and that optimal UA distribution shifted towards increased HTR capacity for mixture-based cycles. The study was concluded with a comparative analysis of the exergy efficiency of pure s-CO_2 and s-CO_2 mixtures in the RBC.

Keywords: Brayton cycle; electrical generation; power systems; s-CO_2 mixtures.

Academic Editor: Firstname Lastname

Received: date
Revised: date
Accepted: date
Published: date

Citation: To be added by editorial staff during production.

1. Introduction

Supercritical carbon dioxide (s-CO_2) Brayton power cycles have gained significant attention in recent decades as a promising alternative to conventional steam Rankine cycles for power generation [1,2,3]. By operating the working fluid above its critical point (critical temperature ≈31°C, critical pressure ≈7.4 MPa), s-CO_2 cycles can achieve high thermal efficiencies (often exceeding 50% at moderate turbine inlet temperatures) [1]. They also feature a compact turbomachinery size and high-power density, owing to the high fluid density in the supercritical state [2]. These advantages make s-CO_2 systems attractive for a range of applications, including next-generation nuclear reactors [3,4,5,6], concentrated solar power (CSP) plants [7,8], and waste heat recovery in industrial processes [9,13]. In particular, the s-CO_2 Brayton cycle's efficiency remains high even at the intermediate heat source temperatures of advanced nuclear and CSP systems, and the

simpler single-phase circuit enables potentially lower cost and smaller footprints than water–steam cycles [2,7,9]. Technology has been extensively reviewed in the literature [2,4,5,6], and several pilot and demonstration projects are underway to validate its performance in practice [8]. However, despite these strengths, certain operational challenges must be addressed before s-CO_2 cycles can realize their full potential across all conditions.

One key challenge arises from the thermophysical characteristics of CO_2 near its critical point. The performance of an s-CO_2 cycle is highly sensitive to the temperature and pressure at the cold end of the cycle (condenser/cooler and compressor inlet) [10,11]. In theory, lowering the compressor inlet temperature should increase the cycle's pressure ratio and thermal efficiency, analogous to how a colder sink boosts a Rankine cycle's efficiency. In practice, however, CO_2's relatively high critical temperature (~31°C) imposes a limit on how much the sink temperature can be reduced [12]. If the ambient heat rejection temperature falls near or below 31°C, the CO_2 in the cooler will approach two-phase conditions, risking condensation or unstable operation at the compressor inlet. Most s-CO_2 systems are therefore designed to maintain the cooler outlet (compressor inlet) just above the critical temperature (typically 32–35°C) to avoid crossing into the two-phase region [12,13,14]. This means that in cold ambient environments – for example, locations with sub-freezing air temperatures or applications with a very low-temperature heat sink – a conventional s-CO_2 Brayton cycle cannot fully capitalize on the cold sink without risking condensation. The net result is a performance penalty in cold conditions: the cycle cannot be optimally cooled, and the compressor may not realize the reductions in work that a colder inlet would otherwise allow. In short, whereas high ambient temperatures (e.g. 40–50°C in desert climates) are known to degrade s-CO_2 cycle efficiency by forcing a higher compressor inlet temperature [12], very low ambient temperatures present the opposite problem of CO_2's phase limitations, effectively constraining the minimum compressor inlet temperature and forfeiting potential efficiency gains. This issue stemming from CO_2's critical-point proximity represents a significant knowledge gap for deploying s-CO_2 cycles in cooler climates or in applications with seasonal ambient swings.

A promising approach to overcome this thermodynamic constraint is to modify the working fluid itself via binary mixtures. Rather than using pure CO_2, the working fluid can be blended with a secondary component to tailor the fluid's critical properties and overall performance [2,14]. By adjusting the mixture composition, it is possible to shift the critical point of the working fluid and alter its thermal behavior in the cycle. This concept is analogous to refrigerant blending in Heating, Ventilation, and Air Conditioning (HVAC) applications and has precedent in power cycles as well: helium–xenon mixtures have been used in closed Brayton cycles to optimize turbomachinery performance [14], and ammonia–water mixtures in Kalina cycles exploit variable boiling properties to improve heat recovery [14]. In the context of s-CO_2 power systems, research in the past decade has increasingly explored CO_2-based binary mixtures as a means to enhance cycle efficiency or extend operability beyond the limits of pure CO_2 [15,16]. Several reviews and comparative studies have categorized CO_2 mixture strategies alongside other cycle improvements [2,7,14,17], underscoring that working-fluid composition adjustment is now recognized as a viable route for performance enhancement.

Early investigations into CO_2-based mixtures for power cycles demonstrated the potential benefits and trade-offs of this approach. For instance, researchers at Sandia National Laboratories conducted one of the first mixture studies on a supercritical CO_2 loop, examining the effect of adding small amounts of various gases (e.g. SF_6, CH_4, N_2, neon, n-butane) on a 50 kW s-CO_2 compressor's performance [18]. Around the same time, Jeong et al. [4,5,6] introduced the idea of tuning CO_2's critical point for better thermodynamic cycle coupling with a sodium-cooled fast reactor, by blending CO_2 with select gases. They tested five candidate additives spanning a range of critical temperatures – namely

cyclohexane, n-butane, isobutane, propane, and hydrogen sulfide (H_2S) – and found that among these, the CO_2/H_2S mixture yielded the highest cycle thermal efficiency [4,5,6]. H_2S, being a "heavier" component with a critical temperature around 100°C, effectively raises the working fluid's critical point, enabling a partial condensation in the cycle and thereby reducing compression work through liquid pumping in a transcritical process. On the other hand, CO_2/propane mixtures were noted to offer superior heat transfer performance and lower pressure drops in heat exchangers [19], owing to propane's favorable thermophysical properties, even if their impact on cycle efficiency was less pronounced than H_2S. These studies suggested that properly chosen additives can improve various aspects of cycle performance, but the optimum choice may depend on whether one prioritizes maximum efficiency or other factors like heat transfer and pressure drop [20,21,22].

More recently, attention has focused on high-critical-temperature additives that deliberately allow condensation at the compressor inlet to boost efficiency. One notable example is the use of titanium tetrachloride ($TiCl_4$) as a CO_2 co-fluid. $TiCl_4$ has an extremely high critical temperature (around 365°C) and was proposed as a means to create a transcritical CO_2 cycle that operates more like a Rankine cycle with a liquid pump. Computational studies by Bonalumi et al. [7] and experimental assessments by Invernizzi et al. [8] showed that adding a small fraction of $TiCl_4$ to CO_2 can increase the cycle's efficiency by several percentage points. In fact, a CO_2–$TiCl_4$ blend was reported to improve Brayton cycle efficiency by up to ~5.5% absolute compared to pure CO_2 [7,8]. Moreover, such heavy-fluid blends were found to mitigate performance degradation under high ambient temperatures: by raising the critical point well above ambient, the cycle can condense and reject heat more effectively even on hot days, avoiding the steep efficiency drop-off pure CO_2 experiences at high sink temperatures [16]. These findings reinforce the idea that altering the working fluid composition can be a powerful tool to tailor cycle behavior to different operating regimes [23,24]. Overall, optimized CO_2-based mixtures have been shown to either increase peak efficiencies or maintain higher efficiencies over a wider range of ambient conditions than the standard pure-CO_2 cycle [15,16]. In other words, mixtures provide an extra degree of freedom in cycle design, potentially extending the operational envelope into conditions that pure CO_2 cannot handle as efficiently [25,26].

Despite the growing body of work on CO_2 mixtures, the majority of studies to date have emphasized heavier additives aimed at high-temperature or high-ambient applications. These heavy additives (with higher critical temperatures than CO_2) enable cycle architectures that include partial condensation, and they tend to yield benefits when the ambient heat sink is relatively warm or when the goal is to maximize absolute efficiency via recuperation and liquid pumping [7,8,16]. In contrast, far less attention has been given to the converse strategy: using low-critical-temperature additives to improve cycle performance in cold ambient conditions. Lighter gases (with lower critical temperatures than CO_2) can depress the critical point of the working fluid mixture, theoretically allowing the cycle to remain supercritical even at much lower sink temperatures. Intuitively, this approach could unlock higher efficiencies in cold environments, since the cycle could operate with a much lower compressor inlet temperature (fully supercritical, single-phase) without encountering two-phase issues. However, previous investigations into light additives have been limited and somewhat inconclusive. In some cases, adding a non-condensable light gas like helium or neon had negligible or even slight negative effects on cycle efficiency at design conditions [16]. For example, Vesely et al. found that small admixtures of low-boiling gases (He, Ar, etc.) provided minimal efficiency improvement in a recompression cycle, primarily affecting the cycle only under off-design scenarios [18]. In other words, the magnitude of benefit likely depends on how far the ambient/cooling conditions deviate below CO_2's natural critical point [16]. It has been posited that the colder the environment (relative to 31°C), the more significant the efficiency gains a

suitably tailored low-critical-point mixture could achieve [16]. This hypothesis, though compelling, remains to be thoroughly tested. To date, there has been no comprehensive study focusing on optimizing s-CO_2 cycle performance specifically for very cold ambient temperatures using light-component mixtures. Most mixture research has targeted improving the base cycle or hot-day operability, leaving a gap in knowledge regarding cold-day or cold-climate operation.

The present study seeks to address this gap by systematically exploring CO_2-based binary mixtures with low-critical-temperature additives as a strategy to enhance recompression Brayton cycle performance in cold ambient conditions. In particular, this work focuses on four candidate additives – methane (CH_4), nitrogen trifluoride (NF_3), carbon tetrafluoride (CF_4), and krypton (Kr) – which were selected for their markedly lower critical temperatures compared to CO_2. All four substances have critical temperatures well below 0°C [27,28,29,30].

Of course, introducing new working fluids also entails practical considerations, particularly with respect to safety and environmental impact [31]. Some prior studies have highlighted the importance of accounting for environmental factors when evaluating alternative working fluids [32,33]. In the present case, each of the candidate additives comes with certain caveats. CH_4 is combustible and has a global warming potential (GWP) as a greenhouse gas, although its atmospheric lifetime is relatively short. NF_3 and CF_4 are chemically inert in the cycle; however, both are extremely potent greenhouse gases if released. For example, NF_3 has an atmospheric 100-year GWP on the order of 17,200 times that of CO_2, and CF_4 around 7,390 times that of CO_2 [33,34]. These values are many times higher even than CO_2 or CH_4, meaning that even a small leakage of NF_3 or CF_4 could offset the CO_2 emissions savings from efficiency gains. Krypton is an inert noble gas with no toxicity or flammability concerns; it has essentially zero direct GWP since it does not absorb infrared radiation. However, Krypton is a rare constituent of air (approximately 1 ppm by volume) and is expensive to procure in large quantities. The use of Kr on an industrial scale would require gas separation infrastructure and careful economic consideration. Considering these issues, the present study not only evaluates the thermodynamic performance of CO_2-based cold-climate mixtures but also discusses the environmental implications and practical viability of each blend. By examining both efficiency gains and potential environmental costs, this study aims to identify which (if any) of these CO_2–based binary mixtures offer a meaningful performance improvement in cold ambient conditions and a reasonable trade-off in terms of safety and sustainability. The results and insights from this work will help guide the development of s-CO_2 Brayton power cycles that can operate efficiently across a broader range of ambient temperatures, including extremely cold environments that were previously considered challenging for pure-CO_2 systems.

2. Methodology

2.1. Cycle Configuration

A recompression Brayton cycle with supercritical CO_2 as the baseline working fluid was modeled [35,36]. The cycle includes: a low-temperature (LT) recuperator and a high-temperature (HT) recuperator, a main compressor and a recompressor, a primary heat source that raises the fluid temperature prior to expansion in a turbine and a cooler that lowers the fluid temperature and pressure after expansion and recuperation, before compression. The pinch points in the LT and HT recuperators were monitored to ensure sufficient temperature differentials for effective heat exchange. The total heat transfer conductance (UA) of each recuperator was set based on design constraints.

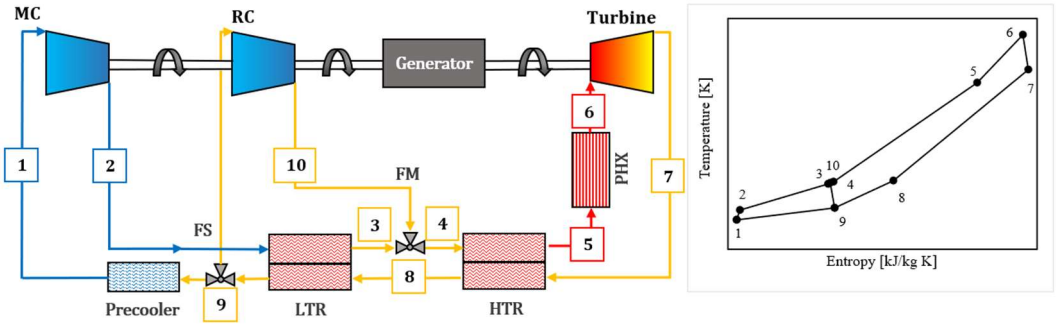

Figure 1. Recompression Brayton power cycle and T-s diagram [35].

2.2. Recompression Brayton Cycle Simulation Methodology

The supercritical CO_2 recompression Brayton (RBC) cycle is modeled using a steady-state, sequential modular simulation strategy. In this approach, each component of the cycle is solved in turn (following the working fluid's flow path) while enforcing conservation laws at defined state points. The RBC configuration features two compressors operating in parallel, where an additional recompressor handles a fraction of the flow that bypasses the precooler. This split-flow arrangement creates a recirculation (recompression) loop, which is closed by mixing the recompressed stream with the main compressor stream upstream of the high-temperature recuperator (HTR). To handle this, recycle loop, a tear stream (the split flow) is chosen, and an iterative solution is applied: the simulation makes an initial assumption for the split fraction (or an intermediate state, such as a recuperator outlet temperature), then repeatedly solves the cycle until the assumption converges to a consistent value within tolerance.

At the start of each simulation, known boundary conditions (e.g. maximum turbine inlet temperature, high and low pressures, ambient cooler temperature) are applied and all cycle state points are initialized. The solver then proceeds sequentially through the components. For example, using the given inlet conditions, the turbine expansion is computed first, yielding the turbine outlet state. Next, the main compressor intake (at the precooler outlet) is compressed to the high pressure, giving the main compressor discharge state. With those results, the high-temperature recuperator is solved using an initial guess for the unknown temperature or flow split that characterizes the recompression loop. Given the HTR's calculated heat transfer, the model then computes the recompressor outlet state (compressing the bypassed fraction) and the low-temperature recuperator (LTR) performance. The two streams (recompressor and LTR outlet) are mixed at common pressure to form a single stream entering the HTR cold side. An iterative loop adjusts the guessed variable (e.g. the recompression mass fraction or the LTR outlet temperature) and repeats the component calculations until the energy balances in the recuperators and the mass split between branches are consistent. This iterative procedure ensures that the recompression loop converges and that both recuperators meet their design conditions (such as matching outlet temperatures or heat duties within a specified residual). The result is a fully converged set of state point properties around the cycle that satisfy all component equations and loop closure requirements.

2.3 Component Modeling

The cycle model encompasses all key components of a recompression Brayton cycle: a turbine, a main compressor, a recompressor, two recuperative heat exchangers (low- and high-temperature recuperators), a primary heat exchanger (heat source), and a precooler (heat sink). Each component is represented by steady-state thermodynamic relationships capturing its performance and limitations.

The **turbomachinery models** (turbine and compressors) employ isentropic efficiency definitions and known pressure ratios. For the turbine, the expansion is assumed adiabatic and isentropic efficiency is used to determine the actual outlet enthalpy from the ideal (isentropic) enthalpy drop. This yields the turbine work output (per unit mass) and the outlet temperature after expansion. Similarly, for both the main compressor and the recompressor, the isentropic efficiency and pressure rise are applied to find the required work input and outlet enthalpy (and temperature) for each compression process. These calculations are enthalpy-based and ensure that the turbine and compressors meet their specified performance (for example, a fixed isentropic efficiency). Mass flow continuity is enforced: the total mass flow through the turbine equals the sum of the flows through the two compressors, and the flow split between the main compressor and recompressor is consistent with the resolved split fraction.

Heat exchangers are modeled by applying energy balances and heat-transfer relationships. The **recuperators (HTR and LTR)** transfer heat between the hot exhaust side and the cooler compressed side of the working fluid. In the simulation, each recuperator is characterized by a specified overall conductance (UA value) or an effectiveness (a measure of heat exchanger performance). A UA-based modeling approach is used here: the heat exchange equations ensure that the heat lost by the hot stream equals the heat gained by the cold stream (assuming no heat loss to the environment, i.e. the units are well insulated). Because the working fluid's heat capacity can vary with temperature, the outlet temperatures of the hot and cold streams are not known explicitly from algebraic formulas and must be determined by solving the coupled energy balance and UA relationship. The simulation iteratively adjusts the estimated outlet temperature on one side of the recuperator until the calculated heat transfer *matches* the specified UA (within a very tight tolerance). In practice, this is done by computing the heat transfer for a trial outlet temperature, evaluating the imbalance or residual (e.g. the difference between required and achieved UA or the energy imbalance), and then using a root-finding method to correct the estimate. A combination of bisection (bracketing) and secant iterations is employed to ensure robust and efficient convergence of this non-linear problem. If the specified UA of a recuperator is effectively zero (below a threshold, e.g. 1×10^{-12}), the component is treated as inactive (bypassed) in the model – meaning no heat is exchanged in that recuperator. This allows the code to seamlessly handle configurations where one of the recuperators is omitted by simply setting its UA to a negligible value.

The **primary heat exchanger** (sometimes called the hot source or heater) adds thermal energy from an external source to the working fluid, raising its temperature to the turbine inlet set point. In the model, this component is simulated by an energy balance that brings the fluid from the HTR outlet up to the turbine inlet temperature. The added heat (cycle heat input) is calculated as the mass flow times the enthalpy rise of the fluid. A pressure drop can be assigned to the primary heater as well, reducing the pressure from the compressor discharge to the turbine inlet (if specified, this can be a fixed pressure decrement or a fraction of the inlet pressure).

Finally, the **precooler** rejects waste heat from the working fluid to an ambient sink (for instance, cooling water or air) at the low-temperature end of the cycle. The precooler cools the fluid from the LTR outlet down to the compressor inlet temperature. Its modeling involves an energy balance that determines the removed heat duty and ensures the fluid reaches the desired low temperature before entering the main compressor. A pressure drop may also be applied across the precooler. Both the primary heater and precooler are assumed to operate under steady conditions, with any heat losses to the surroundings neglected or encompassed in the specified performance. Together, these component models form a complete set of equations that describe the thermodynamic transformation of the working fluid around the cycle.

2.4 Performance Calculation

Once the thermodynamic state points are fully resolved, the overall performance of the recompression Brayton cycle is assessed by evaluating the component-specific and cycle-wide metrics. The **specific work output** of the turbine is computed using the isentropic expansion model, corrected by the turbine isentropic efficiency (η_{turb}):

$$w_{turb} = \eta_{turb} \cdot (h_{turb,in} - h_{turb,out,isentropic}) \quad (1)$$

Similarly, the **specific work input** for both the main compressor and recompressor is evaluated using:

$$w_{comp} = \frac{h_{comp,in} - h_{comp,out,isentropic}}{\eta_{comp}} \quad (2)$$

These values are multiplied by the respective mass flow rates to calculate the component-wise **power outputs and consumptions:**

$$\dot{W}_{turb} = \dot{m}_{turb} \cdot w_{turb} \quad (3)$$

$$\dot{W}_{MC} = \dot{m}_{MC} \cdot w_{MC} \quad (4)$$

$$\dot{W}_{RC} = \dot{m}_{RC} \cdot w_{RC} \quad (5)$$

The **total net power output** is therefore:

$$\dot{W}_{net} = \dot{W}_{turb} - |\dot{W}_{MC} + \dot{W}_{RC}| \quad (6)$$

where:

$$\dot{m}_{RC} = \gamma \cdot \dot{m}_{turb} \quad (7)$$

$$\dot{m}_{MC} = \dot{m}_{turb} - \dot{m}_{RC} \quad (8)$$

The **thermal efficiency of the cycle** is defined according to the first law of thermodynamics as the ratio of the net power output to the heat input delivered in the primary heat exchanger (PHX):

$$\eta_{th,cycle} = \frac{\dot{W}_{net}}{\dot{Q}_{PHX}} \quad (9)$$

where the heat duty in the PHX is:

$$\dot{Q}_{PHX} = \dot{m}_{turb} \cdot (h_{PHX,out} - h_{PHX,in}) \quad (10)$$

For the recuperative heat exchangers (HTR and LTR), the **heat transfer rate** is determined by the energy balance between the hot and cold streams:

$$\dot{Q}_{HX} = \dot{m}_{hot} \cdot (h_{hot,out} - h_{hot,in}) \quad (11)$$

The corresponding **UA evaluation** utilizes the logarithmic mean temperature difference (LMTD) method:

$$\dot{Q}_{HX} = UA \cdot \Delta T_{lm} \quad (12)$$

$$\Delta T_{lm} = \frac{(T_{h,in} - T_{c,out}) - (T_{h,out} - T_{c,in})}{\ln\left(\frac{T_{h,in} - T_{c,out}}{T_{h,out} - T_{c,in}}\right)} \quad (13)$$

where **UA** is iteratively adjusted to meet the specified performance criteria, using a combination of bisection and secant methods, with convergence achieved when the residual is below a defined tolerance:

$$\frac{|Residual_{HX}|}{UA_{target}} < 1 \cdot 10^{-12} \tag{14}$$

Furthermore, the **recuperator effectiveness** (ε_{HX}) is computed as:

$$\varepsilon_{HX} = \frac{\dot{Q}_{actual}}{\dot{Q}_{max}} \tag{15}$$

$$\dot{Q}_{max} = C_{min} \cdot (T_{h,in} - T_{c,out}) \tag{16}$$

where:

$$C_{min} = \min(\dot{m}_{hot} \cdot c_{p,hot}, \dot{m}_{cold} \cdot c_{p,cold}) \tag{17}$$

All component **pressure drops** are incorporated into the thermodynamic property calculations, applied either as absolute or relative drops, following:

$$P_{out} = P_{in} - \Delta P_{abs} \tag{18}$$

$$P_{out} = P_{in} \cdot (1 - \Delta P_{abs}) \tag{19}$$

where applicable, when a heat exchanger's UA falls below a predefined negligible threshold ($1 \cdot 10^{-1}$), the component is considered **inactive** and bypassed within the model.

Finally, in scenarios where a **target net power output** is specified, the model adjusts the overall mass flow rate iteratively until the computed net power meets the target within the same numerical tolerance:

$$Residual_{power} = \dot{W}_{net.calculated} - \dot{W}_{net,target} \tag{20}$$

This ensures that the simulated cycle performance reflects both the specified design point and the thermodynamic behavior of the working fluid under the given conditions, capturing the complex interplay of heat exchanger performance, compressor work, turbine expansion, and system irreversibilities.

The exergetic analysis was conducted in accordance with the relevant equations pertaining to the Second Law of Thermodynamics [37]. Furthermore, the assumption of a steady-state and adiabatic system was made. The exergy balance is expressed in equation (21).

$$0 = \dot{E}_Q - \dot{E}_W - \dot{E}_D + \sum \dot{m}_{in} \cdot e_{in} - \sum \dot{m}_{out} \cdot e_{out} \tag{21}$$

where the $\dot{E}_Q$ denotes the exergy rate of the heat transfer, the $\dot{E}_W$ is the exergy rate of the work, the $\dot{E}_D$ signifies the exergy destruction rate, and e is the specific exergy. The specific exergy and exergy values at each state point (i) of the cycle are calculated by equations (22) and (23), respectively.

$$e_i = (h - h_o) - T_o \cdot (s - s_o) \tag{22}$$

$$\dot{E}_i = \dot{m} \cdot e_i \tag{23}$$

The following expressions provide a quantitative representation of the exergetic efficiency of the individual components that constitute the given cycle [38]:

$$\eta_{ex,turb} = \frac{\dot{W}_{turb}}{\dot{m}_{turb} \cdot (e_6 - e_7)} \tag{24}$$

$$\eta_{ex,MC} = \frac{\dot{m}_{MC} \cdot (e_1 - e_2)}{\dot{W}_{MC}} \tag{25}$$

$$\eta_{ex,RC} = \frac{\dot{m}_{RC} \cdot (e_9 - e_{10})}{\dot{W}_{RC}} \tag{26}$$

$$\eta_{ex,HTR} = \frac{(e_5 - e_4)}{(e_7 - e_8)} \tag{27}$$

$$\eta_{ex,LTR} = \frac{(e_3 - e_2)}{(e_8 - e_9)} \tag{28}$$

The exergy efficiency of the cycle is defined as the ratio of thermal efficiency to the Carnot efficiency of the cycle [37,39].

$$\eta_{ex,cycle} = \frac{\eta_{th,cycle}}{\eta_{Eq-Carnot}} \tag{29}$$

The value of $\eta_{Eq-Carnot}^{dis}$ represents the equivalent Carnot efficiency of the cycle [37,39,40,41,42]. This can be calculated using the equation (30).

$$\eta_{Eq-Carnot} = 1 - \frac{T_{rej}^{dis}}{T_{abs}^{dis}} \tag{30}$$

In this equation (30), T_{rej}^{dis} denotes the heat rejection temperature and T_{abs}^{dis} signifies the temperature at which heat is absorbed during the cycle in the discharge stage. The values of these temperatures are determined by means of the following equations:

$$T_{rej} = \frac{\int_{8r}^{5} T \cdot ds}{s_5 - s_{8r}} \tag{31}$$

$$T_{abs} = \frac{\int_{5}^{6} T \cdot ds}{s_6 - s_5} \tag{32}$$

The Second Law of Thermodynamics also allows quantifying the effect that irreversibilities in heat transfer processes or fluid flow throughout a cycle have on the overall performance of the cycle [40]. This necessitates the enhancement of the preceding concept of an equivalent Carnot cycle, as outlined in equation (30), to the subsequent equation:

$$\eta_{th} = \eta_{Eq-Carnot} - \frac{T_{rej} \cdot \dot{\sigma}_{total}}{\dot{Q}_{PHX}} \tag{33}$$

In order to determine the exergy destruction rate of the components of the examined cycle, the following equations are employed [38].

$$\dot{E}_{D,turb} = \dot{m}_{turb} \cdot (e_6 - e_7) - \dot{W}_{turb} \tag{34}$$

$$\dot{E}_{D,MC} = \dot{m}_{MC} \cdot (e_1 - e_2) - \dot{W}_{MC} \tag{35}$$

$$\dot{E}_{D,RC} = \dot{m}_{MC} \cdot (e_9 - e_{10}) - \dot{W}_{RC} \tag{36}$$

$$\dot{E}_{D,HTR} = \dot{m}_{turb} \cdot \big((e_4 - e_5) + (e_7 - e_8)\big) \tag{37}$$

$$\dot{E}_{D,LTR} = \dot{m}_{turb} \cdot (e_2 - e_3) + \dot{m}_{MC} \cdot (e_8 - e_9) \tag{38}$$

342

2.5 Fluid Blends Properties 343

The performance of supercritical CO_2 Brayton cycle is highly sensitive to the thermophysical properties of the working fluid, particularly near the critical point. This section presents a comparative analysis of four binary mixtures—CO_2/Kr, CO_2/CF_4, CO_2/CH_4, and CO_2/NF_3—selected for their potential to tailor critical properties and improve cycle performance in cold ambient or high-efficiency scenarios. All mixture properties were computed using REFPROP v10, and polynomial regressions were applied to experimental and simulated data to evaluate trends as a function of molar composition. Table 1 summarizes the critical temperature, critical pressure, and critical density of pure components used in the binary mixtures: 344 345 346 347 348 349 350 351 352

Table 1. Pure fluids which are used for mixing with s-CO_2. 353

Working Fluid	Critical Temperature (K)	Critical Pressure (kPa)	Critical Density (Kg/m³)
CO_2	304.13	7377.30	467.60
NF_3	234.00	4460.70	562.47
CF_4	227.51	3750.00	625.70
Kr	209.48	5525.00	909.21
CH_4	190.56	4599.20	162.66

Each additive fluid has a significantly lower critical temperature than CO_2, while critical pressures and densities vary depending on the molecular structure and polarity. The goal of binary mixing is to reduce the pseudo-critical temperature of the resulting blend, shifting it downward to better match cold heat sink conditions without excessively raising compression power. The variation of critical properties with molar concentration of the additive species was systematically modeled, as shown in **Figures 2–5** (from attached graphs). For each binary pair, the critical temperature, critical pressure, and critical density evolve nonlinearly with mixture composition. 354 355 356 357 358 359 360 361

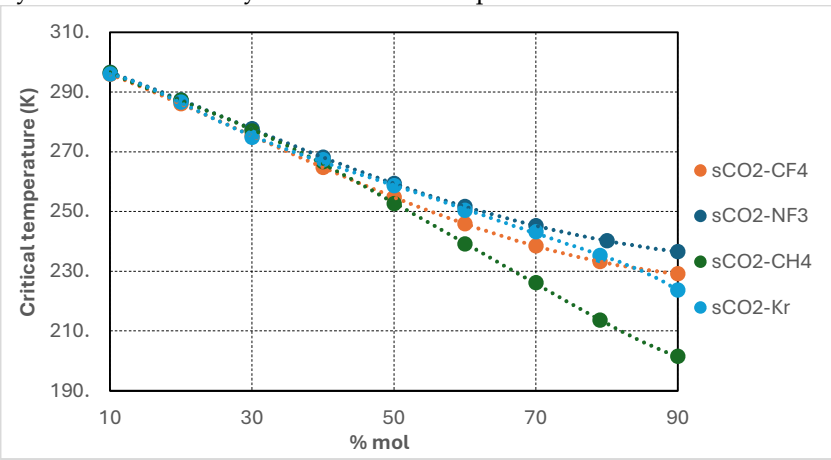

362

Figure 2. Critical temperature vs. blend chemical composition (% molar). 363

Figure 2 illustrates the variation of the critical temperature of supercritical CO_2-based binary mixtures as a function of additive molar concentration, ranging from 10 to 90 mol%. The four investigated mixtures—CO_2/CH_4, CO_2/CF_4, CO_2/NF_3, and CO_2/Kr—demonstrate a consistent decrease in critical temperature with increasing additive content. This trend reflects the dilution effect of the lower-critical-temperature additives on the CO_2-rich mixture. Among the mixtures, CO_2/CH_4 exhibits the most pronounced reduction, achieving critical temperatures as low as approximately 205 K at 90 mol% CH_4. 364 365 366 367 368 369 370

Similarly, CO_2/CF_4 and CO_2/NF_3 mixtures show significant depressions, though less aggressive than CH_4, reaching near 220–230 K at high additive concentrations. The CO_2/Kr mixture displays the most moderate reduction, maintaining critical temperatures above 240 K even at 90 mol% Kr, consistent with Kr's relatively high critical temperature compared to the other additives.

These results confirm that high-additive mixtures effectively lower the mixture's critical point, thereby enabling fully supercritical operation under colder ambient conditions and expanding the applicability range of recompression Brayton cycles in sub-zero environments.

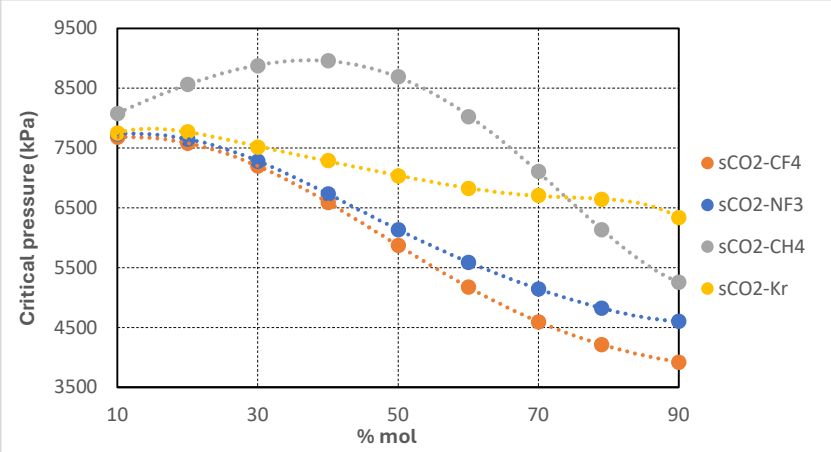

Figure 3. Critical pressure vs. blend chemical composition (% molar).

Figure 3 shows the variation of the critical pressure of supercritical CO_2-based binary mixtures as a function of additive molar concentration. The four studied mixtures—CO_2/CH_4, CO_2/CF_4, CO_2/NF_3, and CO_2/Kr—exhibit distinct behaviors with increasing additive content. For CO_2/CH_4 mixture, the critical pressure initially increases slightly, reaching a maximum at approximately 40 mol% CH_4, before decreasing markedly at higher concentrations. This non-monotonic behavior is characteristic of mixtures where the additive has a significantly lower critical pressure than CO_2 but induces complex phase interactions. Conversely, CO_2/CF_4 and CO_2/NF_3 mixtures show a consistent and nearly linear reduction in critical pressure, with CO_2/CF_4 presenting the most significant drop, falling below 4,000 kPa at 90 mol%. CO_2/Kr mixture displays the least pronounced decrease, maintaining critical pressures above 6,000 kPa across the full range of additive concentrations. These trends have important implications for turbomachinery design in recompression Brayton cycles. Mixtures with lower critical pressures, such as CO_2/CF_4 and CO_2/NF_3 at high additive contents, enable operation at reduced compressor inlet pressures, which can lead to lower specific compression work and smaller compressor pressure ratios. This reduces mechanical stress on compressor components and allows the use of more compact machinery. However, the lower operating pressures also reduce fluid density, particularly at the compressor inlet, which may impact volumetric flow rates and necessitate larger turbomachinery dimensions to handle the same mass flow.

In contrast, mixtures like CO_2/Kr, which retains relatively high critical pressures, will require higher compressor inlet pressures and higher-pressure ratios, leading to greater specific work requirements and more robust compressor designs. The non-monotonic behavior of CO_2/CH_4 mixture demands careful consideration in component sizing and design, as the optimal cycle pressure levels may shift depending on the chosen mixture composition. Overall, the ability to tailor the cycle's critical pressure via mixture composition offers flexibility in turbomachinery optimization, balancing the trade-offs between

pressure ratio, compression work, volumetric flow handling, and component mechanical limits.

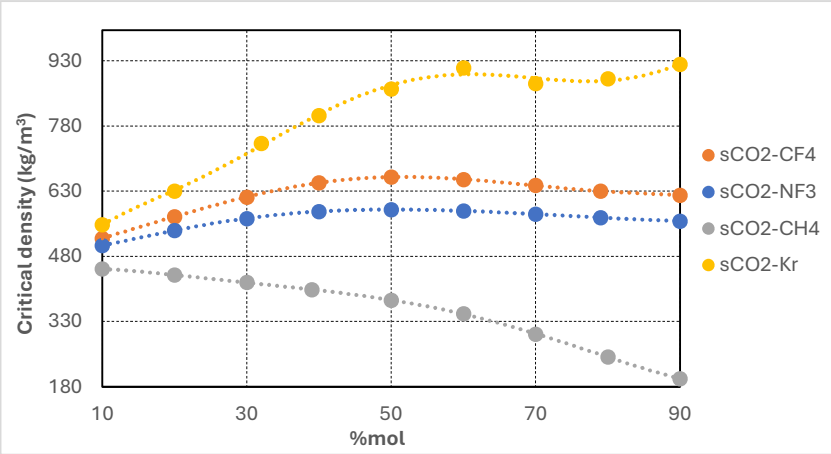

Figure 4. Critical density vs. blend chemical composition (% molar).

Figure 4 presents the variation of the critical density of supercritical CO_2-based binary mixtures as a function of additive molar concentration. The four analyzed mixtures—CO_2/CH_4, CO_2/CF_4, CO_2/NF_3, and CO_2/Kr—exhibit markedly different trends with increasing additive content. CO_2/Kr mixture demonstrates the highest increase in critical density, reaching values above 880 kg/m³ at high Kr concentrations, due to Krypton's inherently high critical density. This trend is favorable for cycle components, as higher working fluid density improves compressor suction conditions, reduces volumetric flow rates, and leads to more compact turbomachinery and heat exchanger designs. This enables more efficient compression stages and smaller equipment footprint. In contrast, CO_2/CH_4 mixture shows a continuous decrease in critical density with increasing CH_4 content, dropping below 200 kg/m³ at 90 mol%. This significant reduction in fluid density presents design challenges, such as larger volumetric flow rates, increased compressor dimensions, and higher flow velocities, which can increase pressure drops in pipelines and heat exchangers. These factors may counteract some of the thermodynamic efficiency gains obtained from lower critical temperatures and pressures, by introducing higher irreversibilities and larger component sizes.

CO_2/CF_4 and CO_2/NF_3 mixtures exhibit moderate increases in critical density at low to intermediate additive contents, peaking around 50 mol%, followed by slight decreases at higher concentrations. This suggests that optimal density values can be achieved at moderate additive levels, balancing fluid properties favorably for both compression work reduction and compact component design. Overall, the trends in critical density have direct implications on power cycle component sizing, mechanical design, and overall system efficiency. Mixtures with higher critical densities (such as CO_2/Kr and CO_2/NF_3 at moderate blends) offer better volumetric efficiencies in compressors, lower pumping power, and reduced pressure drop penalties in heat exchangers, supporting more efficient and compact cycle architectures. Conversely, mixtures that result in low critical densities (notably CO_2/CH_4 rich blends) require careful design considerations to mitigate the adverse effects on component sizing and cycle parasitic losses, despite their potential for enhanced thermodynamic cycle performance at very low ambient temperatures.

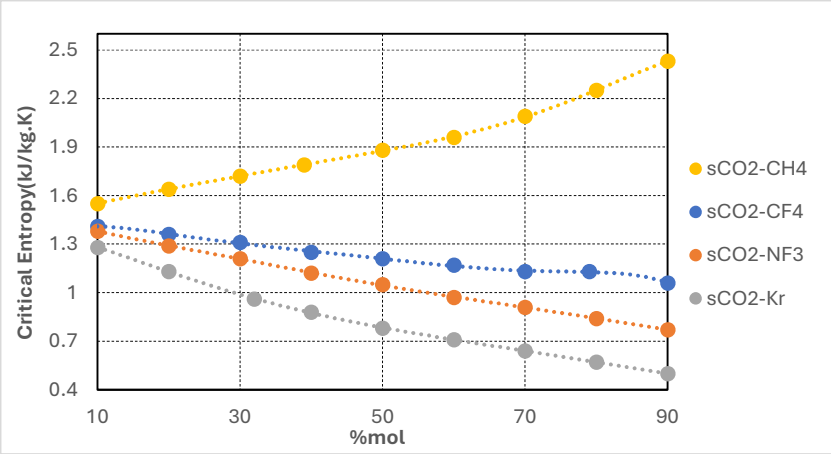

Figure 5. Critical entropy vs. blend chemical composition (% molar).

Figure 5 illustrates the variation of the critical entropy of supercritical CO_2-based binary mixtures as a function of additive molar concentration for CO_2/CH_4, CO_2/CF_4, CO_2/NF_3, and CO_2/Kr systems. The results reveal two distinct trends. CO_2/CH_4 mixture exhibits a monotonic increase in critical entropy, reaching values above 2.4 kJ/kg·K at high CH_4 concentrations. This trend indicates a broadening of the two-phase envelope and reflects increased molecular disorder near the critical point, characteristic of light, highly volatile additives such as methane. In contrast, CO_2/Kr, CO_2/NF_3, and CO_2/CF_4 mixtures show a progressive decrease in critical entropy with rising additive content, with CO_2/Kr mixtures exhibiting the lowest critical entropy values across all concentrations.

From a thermodynamic perspective, critical entropy is an indicator of fluid expansivity and compressibility near the critical point. Mixtures with higher critical entropy, such as CO_2/CH_4, tend to have higher specific volume changes during expansion, potentially increasing turbine enthalpy drops and enabling greater work output. However, this also implies larger volumetric flow rates, which can challenge turbine design and reduce mechanical efficiency if not properly addressed. On the other hand, mixtures with lower critical entropy, such as CO_2/Kr and CO_2/NF_3, display more compact thermodynamic behavior. These fluids tend to have lower expansion ratios and reduced entropy generation, favoring narrower turbine blade designs and potentially lower irreversibilities in expansion stages. Lower entropy values also correlate with steeper isentropic, which can enhance control and stability in cycle operation under varying load or ambient conditions.

Overall, the variation in critical entropy offers insight into how each fluid mixture affects expansion dynamics, entropy generation, and exergy performance. The appropriate selection of a working fluid blend must therefore consider not only efficiency gains due to lower critical temperatures, but also the entropy-related impacts on turbine design, recuperator performance, and cycle control complexity.

2.6 Thermodynamic Modeling Validation

A recompression s-CO_2 Brayton cycle was thermodynamically modeled to assess performance under cold ambient conditions [35, 36], the interface of the SCSP software is presented in **Figure 6**. The cycle includes a main compressor, a recompressor, a single turbine, two recuperative heat exchangers (a low-temperature recuperator, LTR, and a high temperature recuperator, HTR), and a precooler (gas cooler) in a closed-loop configuration. High side and low-side pressures were fixed based on design values, and the flow split to the recompressor was optimized to maximize net cycle efficiency. In the steady-state model, pressures, temperatures, and mass flow rates at all key state points (compressor inlets/outlets, turbine inlet/outlet, recuperator interfaces, etc.) are solved by applying

energy balances and isentropic relations to each component. To obtain accurate thermophysical properties at all states, NIST REFPROP v10 (Reference Fluid Properties database) was integrated with the model [43]. REFPROP v10 provides high-accuracy equations of state for pure CO_2 and mixtures, yielding reliable values of density, enthalpy, entropy, specific heats, and other properties over the relevant range of pressures and temperatures. By using REFPROP's real-fluid property evaluations, the modeling captures real-gas effects especially in the near-critical region and for non-ideal gas mixtures. This ensures that phenomena such as property variation at low temperatures and high pressures, which are critical for s-CO_2 cycles near the critical point, are represented with high fidelity. The use of REFPROP is particularly important for simulating CO_2-based working fluid blends, as mixture-dependent properties (e.g. pseudocritical temperature, mixture heat capacities) are calculated with proven mixture models, improving the realism of the cycle simulations.

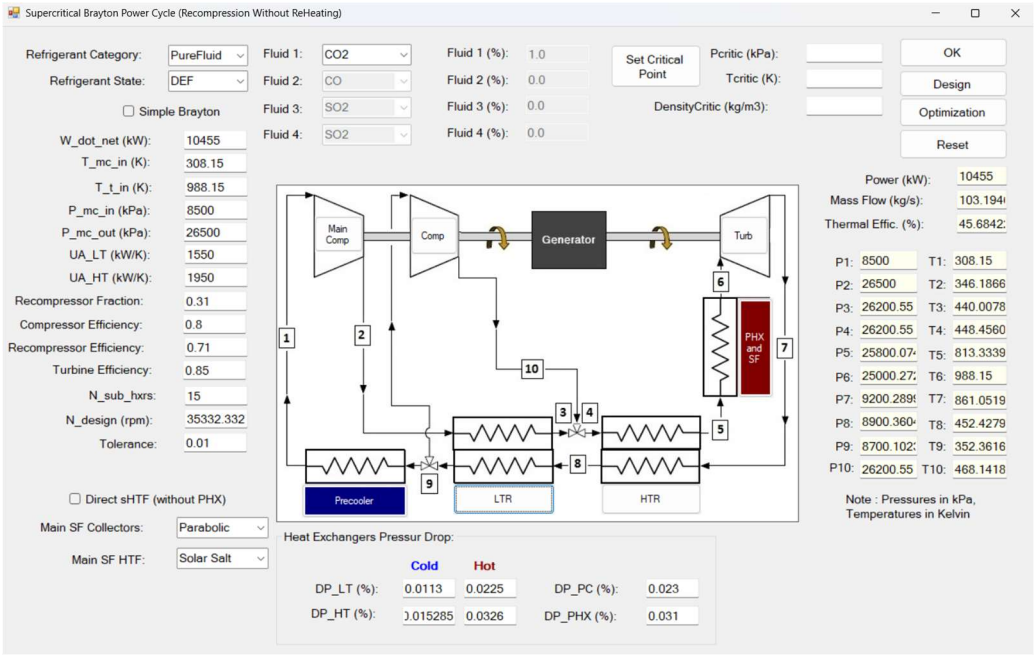

Figure 6. SCSP software [36]. Thermodynamic modelling Verification and Validation base on experimental data provided in 10 MWe STEP pilot plant (Sandia Test Facility) [44].

The validation of the model was undertaken in comparison with experimental data from the 10 MWe STEP pilot plant (Sandia Test Facility, **Figure 7**), which was commissioned in 2024 [44]. This indirect-fired s-CO_2 Brayton facility – the largest of its kind – provided measured temperatures at key state points for a recompression cycle configuration. The predicted cycle temperatures from the SCSP model showed excellent agreement with the STEP pilot data, typically within ±1.2 K of measured values. Such close correspondence between simulation and experiment builds confidence that the thermodynamic equations and property methodologies (REFPROP-based real-gas modeling) accurately capture the behavior of the s-CO_2 cycle. The validated model is therefore a reliable tool for evaluating performance improvements (and potential operational issues) when modifying the working fluid or operating conditions for enhanced cold-condition efficiency.

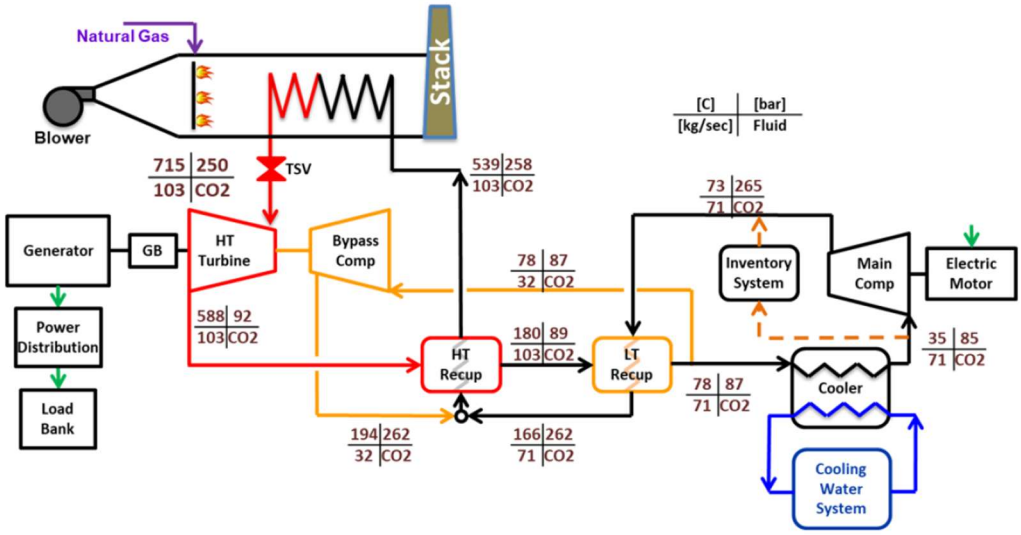

Figure 7. Experimental data from the 10 MWe STEP pilot plant (Sandia Test Facility) commissioned in 2024 [44].

As illustrated in Table 2, a comparison is presented between the results of the study conducted using SCSP software and the work of the Sandia Test Facility, which is used as a reference [44]. The purpose of this analysis is to highlight the relative error that may exist between the two works.

Table 2. Benchmarking and validation of the SCSP software.

Parameter	Reference value [44]	Present work's value	Error (%)
Power Output (MW)	10	10	---
T1 (K)	308.15	308.15	---
T2 (K)	346.15	346.18	0.01
T3 (K)	439.15	440.61	0.33
T4 (K)	No data	448.36	--
T5 (K)	812.15	812.66	0.06
T6 (K)	988.15	988.15	---
T7 (K)	861.15	861.05	0.01
T8 (K)	453.15	453.01	0.03
T9 (K)	351.15	351.21	0.02
T10 (K)	467.15	467.23	0.02
P1 (MPa)	8.50	8.50	--
P2 (MPa)	26.50	26.50	--
P3 (MPa)	26.20	26.20	--
P4 (MPa)	26.20	26.20	--
P5 (MPa)	25.80	25.80	--
P6 (MPa)	25.00	25.00	--
P7 (MPa)	9.20	9.20	--
P8 (MPa)	8.90	8.90	--
P9 (MPa)	8.70	8.70	--
P10 (MPa)	26.20	26.20	--

2.7 Operating Conditions

The simulations were designed to replicate the operating conditions of the **10 MWe STEP pilot plant** located at **Sandia National Laboratories** [44], thereby ensuring the comparability of the results with established experimental data. Accordingly, the recompression Brayton cycle simulations were conducted under the conditions summarized in **Table 3**. The target net electric power output was set at 10,455 kW, considering a generator efficiency of 96%, which yields an effective net electrical output of 10,036.8 kW delivered to the grid. The turbine inlet temperature (TIT) was fixed at 988.15 K (715 °C), representative of advanced heat source temperatures applicable to concentrated solar power and nuclear applications. The main compressor outlet pressure ($P_{MC,out}$) was set at 26.5 MPa, while the compressor inlet pressure (CIP) was defined as 2 bar above the critical pressure of the working fluid blend. This condition ensured the entire cycle operated strictly under supercritical conditions, avoiding any phase instability risks associated with subcritical operation.

Table 3. Key parameters for s-CO_2 recompression Brayton cycle.

	Parameter	Value	Units
Net power output [44]	$\dot{W}_{net}$	10	MW
Turbine inlet temperature [44]	TIT	988.15	K
Compressor inlet temperature*	CIT	$\gtrsim T_{cr}$	K
Compressor inlet pressure**	CIP	P_{cr} + 2	MPa
Compressor outlet pressure [44]	$P_{MC,out}$	26.5	MPa
Heat exchange conductance for the LTR [44]	UA_{LTR}	1550 → 5250	kW/K
Heat exchange conductance for the HTR [44]	UA_{HTR}	1950 → 5500	kW/K
Turbine isentropic efficiency [45]	η_{turb}	0.85	--
Main compressor isentropic efficiency [45]	η_{MC}	0.80	--
Re-compressor isentropic efficiency	η_{RC}	0.71	--
Generator efficiency	η_g	0.96	--
Recompression Fraction	γ	0.31	--
Pressure drops for LT cold [46]	$\Delta P/P_{LT,cold}$	0.0113	--
Pressure drops for LT hot [46]	$\Delta P/P_{LT,hot}$	0.0225	--
Pressure drops for HT cold [46]	$\Delta P/P_{HT,cold}$	0.015285	--
Pressure drops for HT hot [46]	$\Delta P/P_{LT,hot}$	0.0326	--
Pressure drops for precooler [46]	$\Delta P/P_{PreC}$	0.023	--
Pressure drops for PHX [46]	$\Delta P/P_{PHX}$	0.031	--

* The CIT for the mixtures is just above the critical temperature. ** The CIP is 2 MPa above the critical pressure.

The recuperator conductance (UA) values were initially set according to the STEP pilot plant data [44], with UA_LT (low-temperature recuperator) at 1,550 kW/K and UA_HT (high-temperature recuperator) at 1,950 kW/K. This allocation reflects a deliberate emphasis on enhancing heat recovery at higher temperature differentials via the high-temperature recuperator. Additionally, the UA values were varied parametrically to assess cycle efficiency sensitivity to recuperator performance, always ensuring compliance with pinch-point limitations in both recuperators during the analysis.

The isentropic efficiencies of the turbomachinery components were assigned based on established performance metrics for s-CO_2 Brayton cycles operating under similar

conditions, with values of 71% for the main compressor, 80% for the recompressor, and 85% for the turbine. These figures account for known performance penalties associated with real-fluid effects near the critical point and the practical limitations imposed by machinery scaling.

The recompression fraction was set at 31%, which ensures a significant proportion of the flow bypasses the precooler, thereby increasing the recuperation effectiveness and reducing exergy destruction associated with low-temperature heat rejection.

Pressure drops across all heat exchangers were modeled as relative pressure losses, following typical design practices. For the low-temperature recuperator, the cold side pressure drop was set at 1.13% and the hot side at 2.25% of the respective inlet pressures. For the high-temperature recuperator, cold side and hot side pressure drops were 1.5285% and 3.26%, respectively. The precooler and primary heat exchanger (PHX) were assigned pressure drops of 2.3% and 3.1%, respectively. These values represent the expected flow resistance and frictional losses within each component, which can have a significant impact on cycle performance, particularly under high-density working fluid conditions prevalent in supercritical regimes.

These simulation conditions provide a realistic and robust framework for evaluating the thermodynamic performance and design implications of the **recompression Brayton cycle using CO_2-based mixtures**, capturing the key thermophysical and mechanical constraints encountered in practical large-scale power systems.

2.8 Performance Metrics

The thermodynamic performance of each cycle configuration was evaluated using a set of key metrics:

CIT and CIP. These parameters critically affect the thermodynamic state of the working fluid relative to its critical point. CIT determines the fluid density and specific heat at the compressor inlet, while CIP influences the pressure ratio and phase stability. Together, they govern compressor performance, flow stability, and cycle operability, especially under near critical or subcritical conditions.

Recompression fraction. This dimensionless parameter quantifies the fraction of the total flow that bypasses the low-temperature recuperator and is routed through the recompressor. It is optimized to balance recuperative heat exchange and reduce thermal irreversibilities, significantly impacting the effectiveness of the low-temperature heat recovery process.

UA and pinch point temperature difference: The UA values for both the high-temperature recuperator (HTR) and low-temperature recuperator (LTR) define the thermal conductance of each exchanger and represent design constraints on heat transfer capacity. Pinch point temperature differences represent the minimum temperature approach between hot and cold streams within each recuperator. Small pinch points indicate high heat recovery effectiveness but may require larger or more efficient heat exchangers to avoid thermal bottlenecks.

These metrics collectively capture the thermodynamic efficiency, component performance, and design trade-offs inherent to Brayton cycle operation, and are used to compare the relative effectiveness of different working fluid mixtures under cold ambient conditions.

3. Results and Discussion

3.1. Impact of CO_2-Based Binary Mixtures on RBC Performance under Cold Ambient Conditions

The integration of low-critical-temperature additives into the CO_2 recompression Brayton cycle fundamentally alters the thermodynamic landscape of the cycle,

particularly under cold ambient operating conditions where pure CO_2 systems encounter substantial performance limitations due to proximity to or crossing of the fluid's critical point. The extensive simulation results presented in this study reveal the nuanced effects of such mixtures on the overall cycle performance, encompassing thermal efficiency trends, pinch point evolution within the recuperators, critical pressure and density variations, and the implications for turbomachinery and heat exchanger design. This section comprehensively dissects the obtained numerical data, systematically comparing the four studied CO_2-based binary mixtures—CF_4, CH_4, NF_3, and Kr—across the entire operating envelope, with particular emphasis on their respective thermophysical property influences and the resultant cycle behavior.

3.1.1. Enhancement of cycle thermal efficiency with CO_2/CF_4 mixture

Among the investigated additives, tetrafluoromethane (CF_4) emerges as a highly effective agent for enhancing the thermal efficiency of the recompression Brayton cycle at cold conditions. The numerical results presented in **Figure 8** unequivocally show that as the molar concentration of CF_4 in the working fluid increases, there is a clear and monotonic improvement in cycle efficiency, particularly pronounced at high recuperator conductance ($UA_{Total} > 9{,}750\ kW/K$).

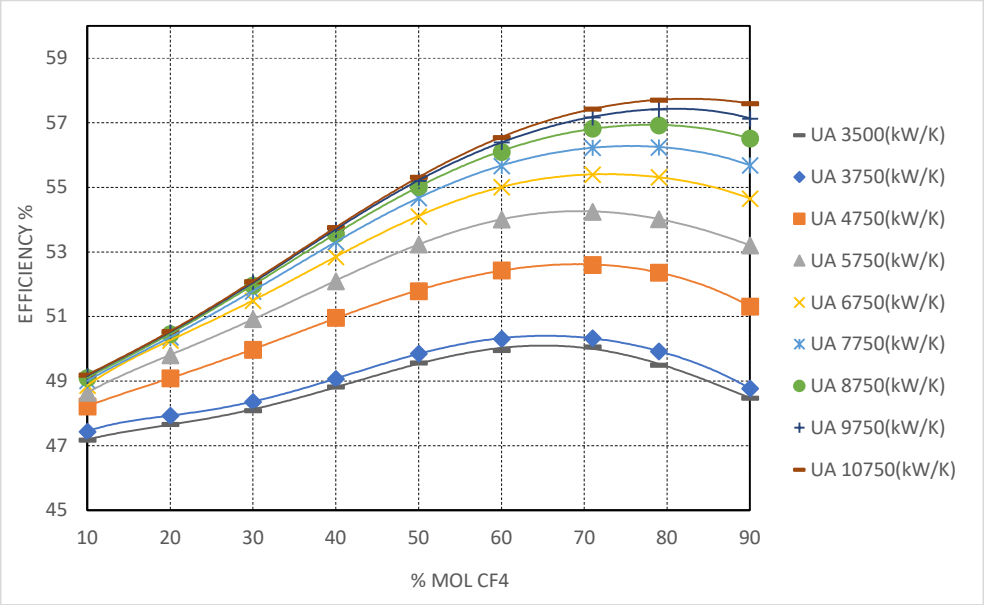

Figure 8. Recompression Brayton cycle thermal efficiency as a function of CF_4 molar concentration for varying total recuperator conductance (UA_{Total}). Efficiency increases significantly with CF_4 content, particularly at higher UA levels, reaching maximum values at ~70–80 mol% CF_4. Efficiency improvements are more sensitive to UA at high additive concentrations due to increased recuperation demands at the low-temperature end.

This behavior is directly attributable to the strong depression of the mixture's critical temperature induced by the addition of CF_4, which possesses a critical temperature of –42.4 °C. As the concentration of CF_4 surpasses 50 mol%, the critical temperature of the mixture falls below –20 °C, effectively eliminating any risk of subcritical operation even at extremely low compressor inlet temperatures (CIT). This capability allows the system to operate fully within the supercritical regime at CITs as low as –40 °C, thereby preserving the favorable thermodynamic characteristics of a dense supercritical fluid while avoiding the substantial performance penalties associated with two-phase flow, high specific work penalties, and compressor surge risks. At a CIT of –42.4 °C and a CF_4 molar fraction of 90%, the cycle achieves a peak thermal efficiency of approximately 54.65%, representing an enhancement of nearly 10 percentage points over the baseline pure CO_2 cycle operating

under the same low CIT conditions. This result highlights the potency of CF_4 in enabling high-efficiency cycle operation in sub-arctic or polar environments, where ambient temperatures frequently fall well below the triple point of CO_2.

The behavior of the high-temperature recuperator (HTR) pinch point in these scenarios is also notably improved compared to pure CO_2 cycles. The inclusion of CF_4 smoothens the temperature glide across the HTR, reducing the risk of sharp pinch points that typically constrain recuperative heat transfer in pure CO_2 systems at low CIT. Nevertheless, the numerical results indicate that to fully capitalize on the improved thermodynamic conditions provided by the mixture, the HTR conductance must be substantially increased. At high CF_4 fractions and CITs approaching -40 °C, the HTR pinch point remains a critical bottleneck, only mitigated when UA_{Total} surpasses 4,750 kW/K.

From a turbomachinery perspective, the reduced mixture critical pressure—falling from approximately 4.74 MPa at 70 mol% CF_4 to near 3.95 MPa at pure CF_4—enables operation at lower compressor inlet pressures (CIP), which directly reduces the specific compressor work and increases the turbine expansion ratio. This thermodynamic advantage is particularly desirable as it enhances the net cycle efficiency and provides greater operational flexibility in compressor design. However, the increase in fluid density at these conditions also necessitates careful consideration of compressor volumetric flows and may impose additional mechanical design challenges, particularly in ensuring adequate sealing and compression ratios at relatively low pressures and temperatures.

3.1.2. Superior efficiency gains with CO_2/CH_4 mixture and challenges in turbomachinery integration

Methane (CH_4) emerges as the most effective additive among the studied candidates in terms of pure cycle thermal efficiency enhancement. The simulation data (**Figure 9**) demonstrate that the CO_2/CH_4 mixtures consistently outperform the other blends, achieving cycle efficiencies exceeding 58% at 90 mol% CH_4 and high UA_{total} values.

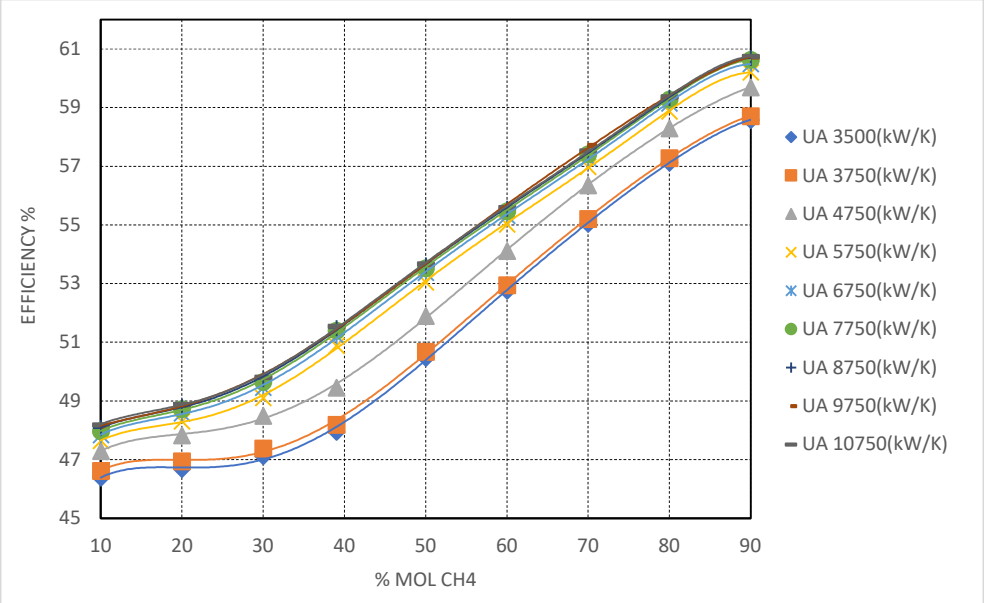

Figure 9. Recompression Brayton cycle thermal efficiency as a function of CH_4 molar concentration for varying UA_{Total}. CH_4-rich mixtures exhibit the highest cycle efficiency improvements among the studied blends, with efficiencies around 60% at 90 mol% CH_4 and high UA. The efficiency sensitivity to UA is most pronounced at high CH_4 fractions and low CIT conditions, highlighting the need for increased HTR conductance

This remarkable performance is fundamentally linked to CH_4's low critical temperature (–82.6 °C or 190.6 K), which, when introduced into the mixture even at moderate

concentrations, sharply lowers the mixture's critical point, ensuring supercritical operation across a vast range of cold CIT scenarios. As with CF_4, this behavior enables the cycle to avoid two-phase flow regimes and associated performance penalties. However, the magnitude of the efficiency gain is significantly more pronounced with CH_4 mixtures, owing to the compound effect of reduced compressor inlet temperatures and expanded turbine pressure ratios facilitated by mixture critical pressures (approaching 7.3 MPa at 70% CH_4 and falling below 5. MPa at higher CH_4 fractions). The enhanced cycle performance of CH_4 mixtures is also tightly coupled to the recuperator performance. The data reveal that the efficiency gains achieved with CH_4-rich mixtures are highly sensitive to the HTR conductance, with the most pronounced benefits only realized at UA_{Total} levels exceeding 5,750 kW/K. This is due to the exacerbated temperature glide across the HTR at very low CITs, which demands aggressive recuperative heat transfer capacity to avoid efficient penalties associated with high pinch points. At lower UA_{Total} levels, the pinch point becomes the dominant constraint, suppressing the thermodynamic advantages conferred by the mixture.

Nevertheless, the superior thermodynamic performance of CH_4 mixtures comes with significant turbomachinery challenges. The low critical pressure and, more critically, the significantly lower fluid densities at the relevant operating conditions (compared to CF_4 or NF_3 mixtures) impose substantial volumetric flow penalties on the compressor. The simulation results show that at high CH_4 contents and low CIT, the compressor volumetric flow can increase by up to 50% compared to pure CO_2 cycles, necessitating larger compressor stages, increased impeller diameters, or multi-stage compression strategies to maintain acceptable compression ratios and efficiencies. Furthermore, the lower fluid densities also impact turbine design, requiring larger flow passages and possibly leading to lower stage efficiencies due to increased tip leakage and off-design operation risks. These design implications necessitate a holistic approach in system integration, ensuring that the gains in cycle efficiency are not negated by practical limitations in turbomachinery scaling or operational stability.

From a heat exchanger perspective, while the smoother temperature glide of CH_4-rich mixtures alleviates some of the extreme pinch point issues encountered in pure CO_2 systems, the results still underscore the necessity of over-sizing the HTR and, to a lesser extent, the low-temperature recuperator (LTR) to fully leverage the thermodynamic benefits. This consideration is critical in system optimization, as the capital costs associated with larger recuperators may offset the gains in cycle efficiency if not carefully balanced.

Overall, while CH_4 mixtures present the highest potential in terms of cycle thermal efficiency under cold ambient conditions, their practical implementation will require significant adaptations in both heat exchanger and turbomachinery design to accommodate the altered fluid properties and flow dynamics inherent to these mixtures.

3.2. Cycle Optimization through Critical Pressure Management and Turbomachinery Implications

Expanding upon the previous discussion, the critical pressure management aspect of the recompression Brayton cycle design emerged as a decisive factor for achieving optimal performance with CO_2-based binary mixtures, particularly in sub-zero environmental scenarios. The reduction in critical pressures, coupled with the enhanced flexibility provided by the lower critical temperatures, resulted in a comprehensive reshaping of the compressor inlet operating window and associated turbomachinery sizing considerations. These thermodynamic trends observed in CF_4 and CH_4 mixtures are quantitatively supported by **Figures 8** and **9**, which not only depict the efficiency improvements but also infer the indirect impacts on turbomachinery operating windows, as higher efficiencies correlate

with more favorable turbine expansion ratios and lower specific compressor work at reduced pressures.

For CF_4-rich blends, the decrease in critical pressure was the most dramatic among the studied additives, with the critical pressure plummeting to approximately 3.95 MPa at pure CF_4 conditions. These substantial decreases opened avenues for significant compressor work reductions as the inlet pressure could be safely lowered without encountering two-phase risks, which is impossible with pure CO_2 at equivalent CIT levels. Additionally, the dense phase behavior at these lower pressures, despite the decrease in density relative to pure CO_2, still maintained acceptable levels of volumetric efficiency due to CF_4's inherent high density, especially under supercritical conditions.

Conversely, the CH_4-based mixtures, while offering superior critical temperature depression and associated efficiency gains, exhibited a more modest reduction in critical pressure, bottoming at approximately 5.4 MPa for CH_4 mole fractions of 90%. This more limited pressure reduction was, however, accompanied by a sharper drop in density due to the gaseous nature of methane even under supercritical regimes. Consequently, while the thermodynamic cycle efficiency was maximized, the compressor volumetric flow rates were substantially increased, imposing the need for considerable redesign of the compressor stages, including larger impeller diameters and more robust volumetric flow management strategies. This underscores the delicate balance between cycle thermal gains and mechanical feasibility in cycle integration.

NF_3 and Kr mixtures displayed intermediary behaviors. NF_3, owing to its molecular weight and thermophysical properties, achieved a moderate reduction in critical pressure down to about 4.6 MPa at pure NF_3 conditions, which, while less pronounced than CF_4 or CH_4, nonetheless provided measurable compressor work reductions. Importantly, NF_3's high fluid density in the supercritical phase ensured that the required compressor volumetric capacities remained close to those of CO_2, thereby simplifying turbomachinery adaptation compared to CH_4-rich blends.

Kr-based mixtures, while providing the least reduction in critical pressure (staying above 5.67 MPa even at 100% Kr), nonetheless offered a noteworthy advantage from a volumetric flow perspective. The high molar mass and exceptional density of Kr resulted in minimal expansion of the volumetric flow rates at the compressor inlet, making these mixtures the most compatible with existing CO_2-based turbomachinery designs. Despite this mechanical compatibility, the limited critical temperature and pressure depression translated into smaller efficiency gains, as will be thoroughly analyzed in subsequent comparative sections.

Thus, from an integrated system design standpoint, CF_4-rich mixtures appeared as the most balanced choice, offering significant efficiency improvements alongside manageable turbomachinery requirements. CH_4 mixtures, while thermodynamically superior, imposed the highest demands on compressor design, while NF_3 and Kr offered intermediary options suitable for applications where moderate efficiency gains were acceptable in exchange for reduced system complexity and easier retrofitting.

3.3. Recuperator Performance Optimization and Sensitivity to UA

Another pivotal aspect analyzed across all the mixtures was the recuperator performance, specifically the sensitivity of cycle efficiency to the total recuperator conductance (UA_{Total}), which varied from 3,500 kW/K up to 10,750 kW/K in the simulations. The results consistently indicated that all studied mixtures exhibited a strong dependence on the recuperator sizing, particularly under cold CIT scenarios.

At lower UA_{Total} values, the cycle efficiency was severely constrained by the recuperator pinch points, particularly at the low-temperature recuperator (LTR) cold end (T9–T2). This effect was more pronounced in mixtures such as CH_4 and CF_4, where the coldest

CIT conditions imposed extreme demands on the LTR. The high degree of recuperation required to preheat the fluid sufficiently prior to entering the main compressor became limited by the LTR pinch point, with temperatures approaching sub-ambient levels, exacerbating the logarithmic mean temperature difference (LMTD) constraints and pushing the system into diminishing returns territory.

As UA_{Total} increased, the recuperator's ability to handle these constraints improved markedly. Particularly, when UA_{Total} exceeded 7,750 kW/K, the gains in cycle efficiency became increasingly linear with respect to further UA increases. For instance, at UA_{Total} of 5,750 kW/K, the CO_2–CH_4 blend at 90% CH_4 content reached cycle efficiencies above 60%, showcasing the pivotal role of heat exchanger optimization in unlocking the full potential of these fluid mixtures.

However, this aggressive recuperator sizing was not equally beneficial across all mixtures. For Kr-based mixtures, the efficiency gains plateaued much earlier, with limited improvements beyond UA_{Total} of 3500 kW/K. This phenomenon is attributed to Kr's inherently higher specific heat and density, which reduces the recuperator's heat duty requirements compared to other mixtures. This observation suggests that for Kr-based cycles, the design of recuperators could be optimized for lower conductance without substantial efficiency penalties, providing a cost advantage in systems where Kr is the preferred additive.

For NF_3-based mixtures, an intermediary behavior was observed. The efficiency gains with UA_{Total} scaled progressively up to approximately 8,750 kW/K, as depicted in **Figure 10**, beyond which the marginal gains diminished, indicating an optimal recuperator conductance range for these blends. The HTR pinch point for NF_3 mixtures remained more manageable compared to CH_4 and CF_4 systems, thanks to NF_3's fluid properties that allowed more favorable heat exchange at the cold end without incurring extreme pinch point penalties.

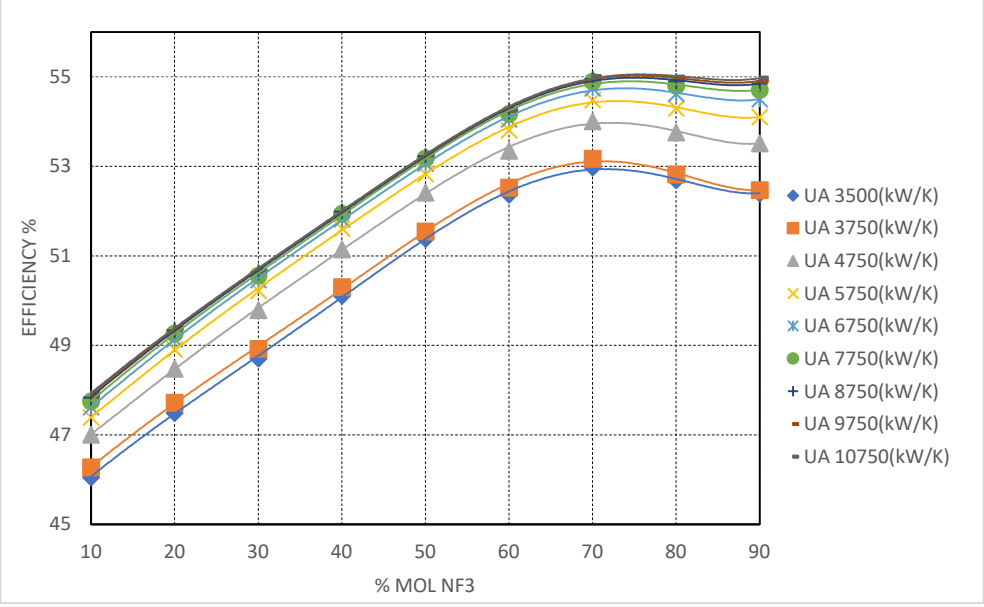

Figure 10. Recompression Brayton cycle thermal efficiency as a function of NF_3 molar concentration for varying UA_{Total}. NF_3-containing mixtures show robust efficiency improvements, achieving peak efficiencies around 54.5% at ~70 mol% NF_3. While gains are lower compared to CH_4 and CF_4 mixtures, the trends confirm NF_3's effectiveness in extending the operational range of the cycle to moderate sub-zero CIT conditions.

This UA sensitivity analysis further highlighted the fact that the high-temperature recuperator (HTR) dominated the cycle performance under cold CIT conditions, with the

low-temperature recuperator (LTR) playing a secondary role. The required UA_HT to mitigate the cold-end pinch was significantly higher in CH_4- and CF_4-rich blends, often exceeding 5,000 kW/K, while Kr and NF_3 mixtures could achieve acceptable pinch management with UA_HT as low as 3,500–4,000 kW/K.

3.4. Comparative Evaluation of Mixture Performance and Operational Trade-Offs

A holistic comparative evaluation of the four studied binary mixtures revealed distinct operational profiles and trade-offs, which are essential for guiding working fluid selection based on specific application requirements.

3.4.1. CO_2/CF_4 Mixtures

CO_2/CF_4 mixtures emerged as the most balanced solution for cold climate applications where both high thermal efficiency and mechanical feasibility are priorities. The cycle efficiency reached up to 58% at 70–80 mol% CF_4 under high UA scenarios, see **Figure 8**, outperforming pure CO_2 by approximately 11–12 percentage points. Importantly, the high density of CF_4 ensured that compressor volumetric flows, while higher than pure CO_2, remained within the practical limits of current turbomachinery capabilities. Additionally, CF_4's compatibility with existing s-CO_2 cycle hardware, due to its favorable thermophysical properties (moderate critical pressure, high density, low viscosity), positioned these mixtures as a strong candidate for retrofitting existing systems to operate in colder climates without necessitating complete redesign of major components.

3.4.2. CO_2/CH_4 Mixtures

CO_2/CH_4 mixtures demonstrated the highest absolute cycle efficiency improvements, exceeding 60% at 90 mol% CH_4 and UA_{Total} above 9,750 kW/K. These unprecedented performance levels confirmed CH_4's unmatched capability to depress the critical temperature deep into the cryogenic range, facilitating entirely supercritical operation even at CITs as low as –70 °C. However, the practical implications of such mixtures were significant. The ultra-low fluid densities at the compressor inlet, coupled with elevated volumetric flow rates, imposed major design penalties on the turbomachinery, requiring larger, heavier, and more complex compressors with increased power consumption for the same mass flow rate. Additionally, the heat exchanger design for these mixtures was the most challenging, demanding the highest UA_{LT} to manage the sharp pinch points at the LTR, particularly under high CH_4 concentrations and extreme sub-zero CITs.

Consequently, while thermodynamically attractive, CO_2/CH_4 mixtures are best suited for specialized applications where maximum efficiency is paramount, and the system can be designed from scratch with appropriately sized and engineered components. This is clearly illustrated in **Figure 9**, where the steep efficiency ascent with CH_4 molar concentration surpasses the performance of all other mixtures, yet concurrently implies the greatest system-level engineering burdens due to the increased volumetric flow rates and heat exchanger sizing requirements.

3.5. Critical Temperature Reduction and Cycle Performance at Sub-Zero Ambient Conditions

The reduction of the working fluid's critical temperature emerges as the central thermophysical parameter influencing the behavior of recompression Brayton cycles under cold ambient conditions. In pure CO_2 cycles, the relatively high critical temperature of 304.13 K (31.0 °C) presents a fundamental barrier to efficient cycle operation at sub-zero conditions. Below this threshold, CO_2 enters the two-phase region at the compressor inlet, triggering substantial inefficiencies due to phase instability, increased compression work, and the impossibility of achieving the necessary supercritical compression and recuperation processes. Binary mixtures of CO_2 with additives like CF_4, CH_4, NF_3, and Kr exhibit significant critical temperature depression, which ensures that the working fluid remains

fully within the supercritical region even at extreme cold compressor inlet temperatures (CIT) as low as -70 °C. This capability is pivotal for extending the operational domain of recompression Brayton cycles in cold climate applications, such as Arctic, Antarctic, and high-altitude deployments, or in off-design scenarios of seasonal low ambient temperatures.

3.5.1 CO_2/CF_4 Mixture

Among the examined mixtures, CO_2/CF_4 exhibits a pronounced reduction in critical temperature, reaching approximately 229.69 K (-43.46 °C) at pure CF_4. The cycle simulations clearly demonstrate that as CF_4 concentration increases, the system benefits from smoother supercritical behavior at lower CIT, avoiding abrupt phase changes and maintaining continuous heat recovery capability through the recuperators. For instance, at 90 mol% CF_4, cycle efficiency peaks at approximately 57.59% under the highest tested UA_{Total} conditions (10,750 kW/K), with pinch-point temperatures in both the HT and LT recuperators minimized. The efficient performance of these mixtures is partially attributed to the higher density and favorable compressibility factor of CF_4-rich blends at low temperatures, which sustains acceptable compressor inlet properties despite the substantial decrease in pressure. Furthermore, the lowered critical pressure (around 3.95 MPa for 100% CF_4) allows the cycle to operate with significantly reduced compressor inlet pressures compared to pure CO_2, further enhancing the turbine expansion ratio and contributing to improved net cycle efficiency. However, designers must account for the increased specific heat capacity of CF_4 mixtures, which elevates recuperation demands and necessitates careful recuperator sizing, particularly at the LT stage.

3.5.2 CO_2/CH_4 Mixture

CO_2/CH_4 mixture stands out for their exceptional cycle efficiency improvements at high CH_4 concentrations. The critical temperature of the mixture drops to 191.91 K (-81.24 °C) for pure CH_4, making these blends uniquely suited for ultra-cold conditions. As CH_4 concentration approaches 90 mol%, cycle efficiency equal to 60%. This represents one of the most dramatic efficiency gains among the studied mixtures, exceeding pure CO_2 by around 15 percentage points in the most favorable configurations. However, this efficiency improvement comes with substantial engineering challenges. CH_4-rich mixtures exhibit significantly lower fluid density at comparable pressures and temperatures, resulting in increased volumetric flow rates through the compressor and recuperators. This requires larger turbomachinery dimensions, greater heat exchanger surface areas, and increased system footprint, which may pose economic and engineering trade-offs for large-scale applications. Nonetheless, the thermodynamic advantage of CH_4 is undeniable in extreme cold environments, where it permits efficient, stable, and high-performance cycle operation across an unprecedented range of ambient conditions.

3.5.3 CO_2/NF_3 Mixture

NF_3-containing mixture offers a balanced performance profile, combining favorable reductions in critical temperature with relatively moderate density penalties. With a critical temperature of 235.65 K (-37.5 °C) for pure NF_3, these mixtures allow the cycle to operate efficiently down to approximately -30 °C CIT without entering the subcritical region. At 70–80 mol% NF_3, cycle efficiencies reach 54.44% under the high UA_{Total} conditions, demonstrating significant gains over pure CO_2, although lower than those achieved with CF_4 or CH_4. From a design perspective, NF_3 mixtures provide a favorable compromise between efficiency, density, and operational stability. The relatively high density of NF_3-rich blends alleviates volumetric flow issues compared to CH_4 mixtures, while still delivering substantial efficiency improvements and manageable pinch-point temperatures in the recuperators. This makes NF_3 an attractive candidate for regions with consistently cold but not extreme sub-zero temperatures, where the mixture's characteristics allow for

system simplification compared to CH_4 while maintaining high thermodynamic performance.

3.5.4 CO_2/Kr Mixture

Krypton, while presenting a relatively limited critical temperature depression compared to the other additives, still contributes to cycle performance improvement by allowing stable supercritical operation at moderate sub-zero CIT (~-50 °C). CO_2–Kr mixtures display the most conservative efficiency enhancements among the studied blends, peaking around 54% at 90 mol% Kr. The main advantage of Kr lies in its high density and minimal impact on mixture compressibility, resulting in manageable volumetric flows and reduced turbomachinery scaling challenges. This is exemplified in **Figure 11**, where the modest but consistent efficiency improvements are depicted, showing Kr-rich mixtures as the least sensitive to UA increases, yet offering stable operational characteristics and turbomachinery compatibility. However, the limited reduction in critical pressure and temperature of Kr-rich mixtures constrains their applicability to moderately cold climates, where the lower gains compared to CH_4 or CF_4 must be carefully weighed against the easier engineering implementation and potentially lower capital costs. Additionally, the high cost and limited availability of Kr may restrict its deployment to niche applications where specific performance or compatibility requirements justify its use.

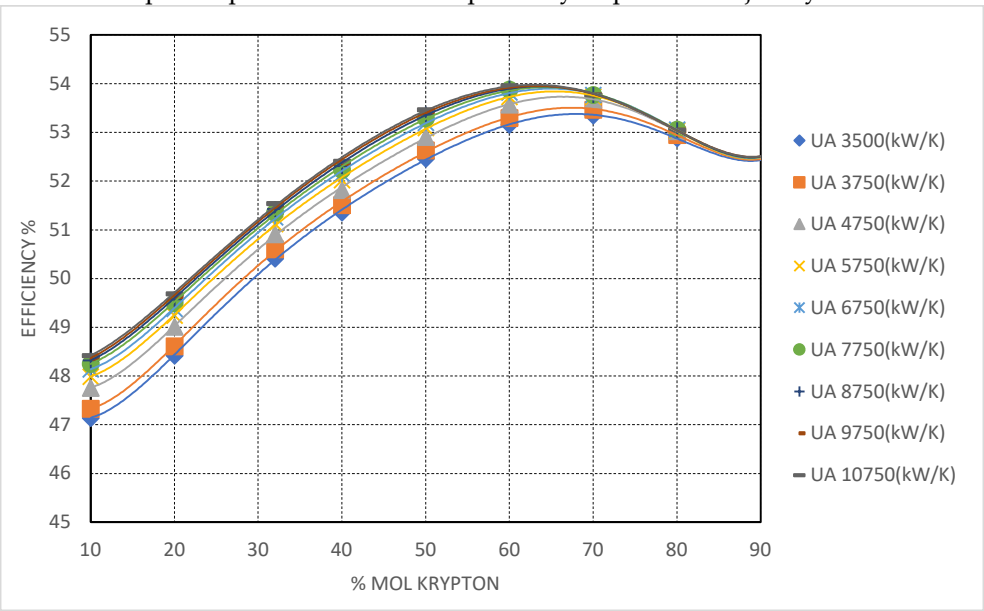

Figure 11. Recompression Brayton cycle thermal efficiency as a function of Kr molar concentration for varying UA_{Total}. CO_2/Kr mixtures provide modest but consistent efficiency enhancements, peaking around 52-53% at 70–80 mol% Kr. Compared to other additives, the efficiency improvements are less sensitive to UA increases, reflecting Kr's higher critical pressure and limited critical temperature reduction capacity.

3.5.5 Comparative Performance Under Various CIT Scenarios

Analyzing the data across all mixtures and CIT scenarios reveals clear trends correlating critical temperature depression with cycle efficiency gains. At CIT values above 0 °C, the differences among mixtures are less pronounced, as most systems operate well within the supercritical region, and pure CO_2 cycles can still achieve acceptable efficiencies (>46%). However, as CIT drops below -10 °C, the benefits of the binary mixtures become increasingly dominant, with CO_2/CH_4 and CO_2/CF_4 maintaining the highest cycle efficiencies and pure CO_2 suffering from severe penalties due to its inability to remain supercritical. Notably, the sensitivity of cycle efficiency to recuperator conductance (UA_{Total}) becomes amplified at lower CITs for all mixtures, as the increased temperature

difference between the recuperator streams demands higher heat exchanger performance to minimize pinch-point limitations. This highlights the necessity for synergistic optimization of fluid composition and heat exchanger design, ensuring that the full benefits of the fluid property modifications are realized without compromising recuperation effectiveness.

3.6 Sensitive Exergy Analysis

The present section is concerned with the examination of the exergy destruction and exergy efficiency of each component of the RBC.

3.6.1 Pure CO_2

The RBC's turbomachine, when the working fluid is pure s-CO_2, exhibits varying exergy efficiencies (see **Figure 12**). The components with the lowest efficiency ratings are the main compressor (MC) and the recompressor (RC). The component that has been demonstrated to exhibit the highest level of efficiency is the high-temperature heat recuperator (HTR).

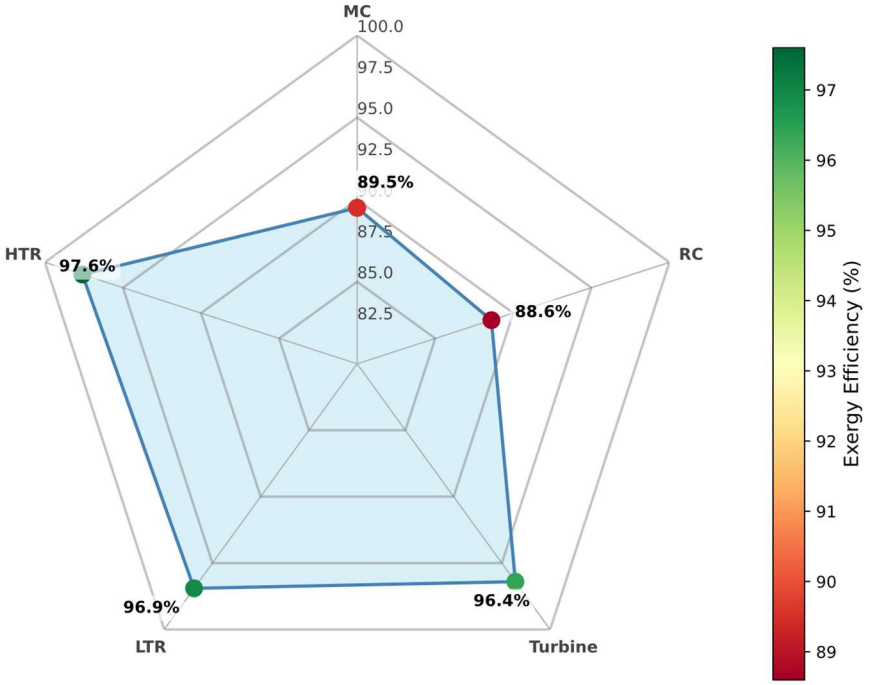

Figure 12. Exergy efficiency with pure s-CO_2

3.6.2 CO_2/CF_4 Mixture

As illustrated in **Figure 13**, the thermodynamic analysis of the cycle components when utilizing CO_2/CF_4 as the working fluid is demonstrated. A percentage comparison of exergy destruction between the pure fluid and the mixture is presented in **Figure 13-a**. It is evident that exergy destruction is reduced exclusively in HTR when the mixture is utilized. Conversely, **Figure 13-b** demonstrates an enhancement in exergy efficiency in both the HTR and the turbine.

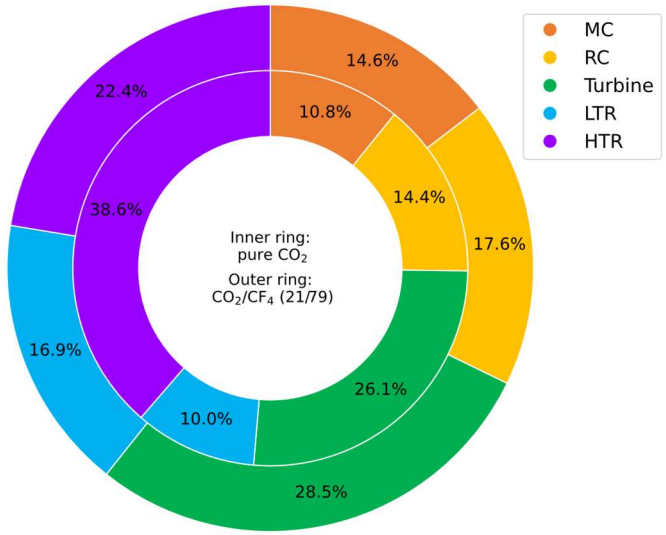

(a)

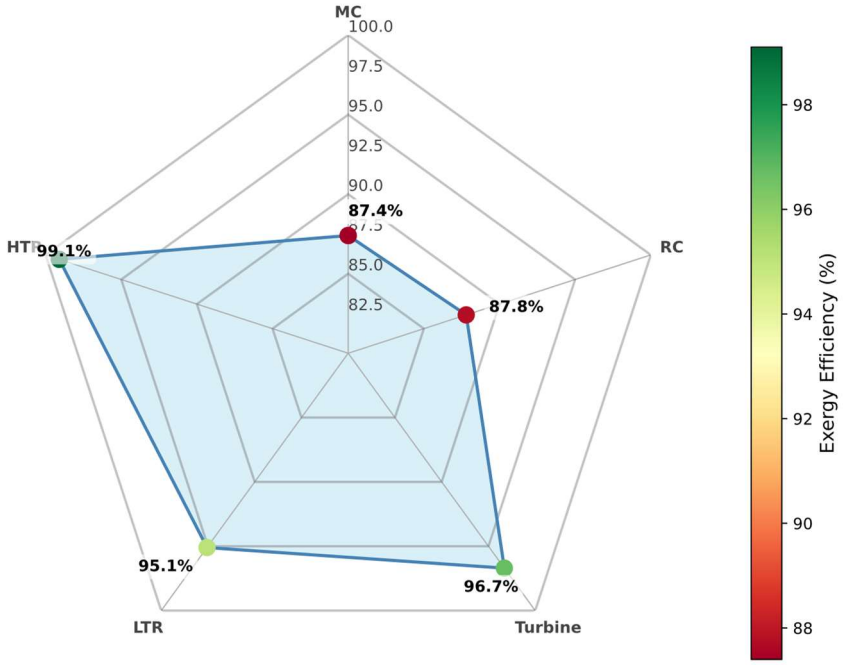

(b)

Figure 13. (a) Exergy destruction and (b) Exergy efficiency with CO_2/CF_4 mixture.

3.6.3 CO_2/CH_4 Mixture

The mixture containing CH_4 has been shown to generate greater exergy destruction in all components except the HTR, whose efficiency is approximately 11% lower (see **Figure 14-a**). In addition, the mixture exhibits reduced exergy efficiency in all components except for the component HTR, which demonstrates 1% higher efficiency (see **Figure 14-b**).

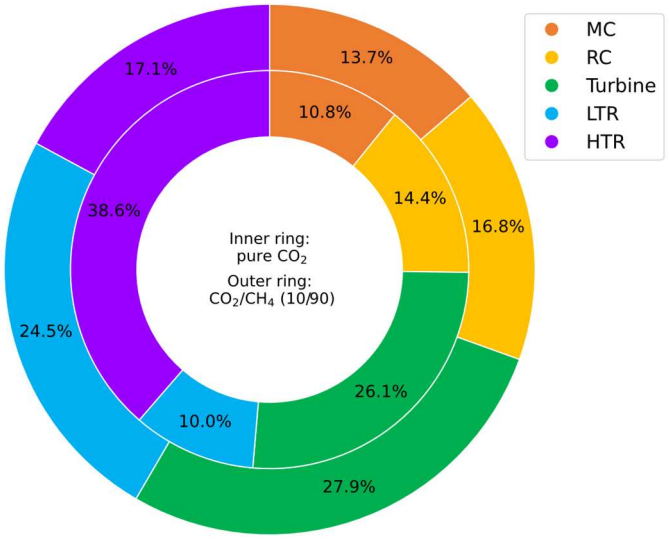

(a)

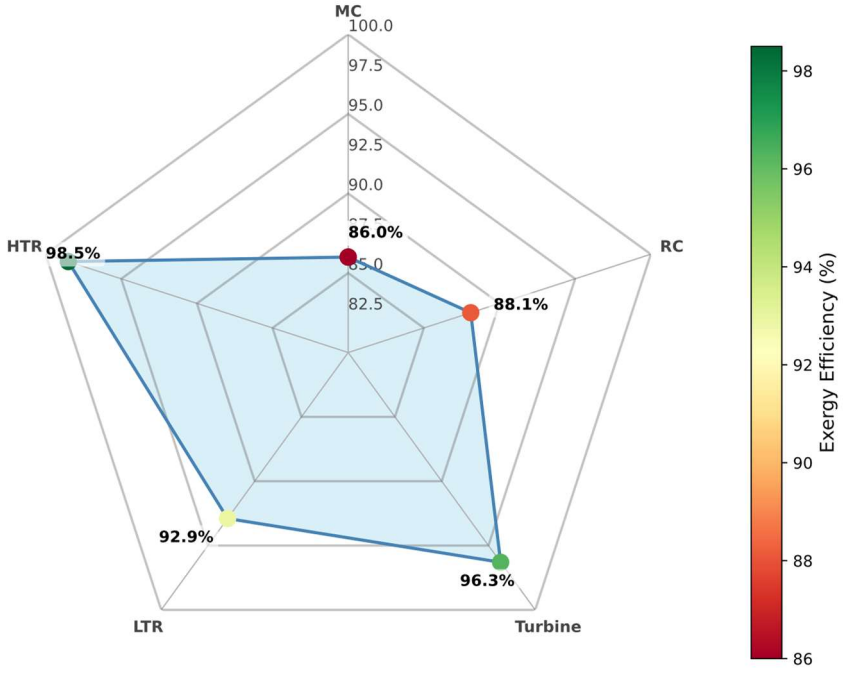

(b)

Figure 14. (a) Exergy destruction and (b) Exergy efficiency with CO_2/CH_4 mixture.

3.6.4 CO_2/NF_3 Mixture

In the CO_2/NF_3 mixture, exergy destruction in HTR is approximately 17.5% lower, but in the turbine, it is 6.5% better. A thorough analysis of the exergy efficiency of the components reveals that there is only a marginal improvement in HTR compared to the pure fluid.

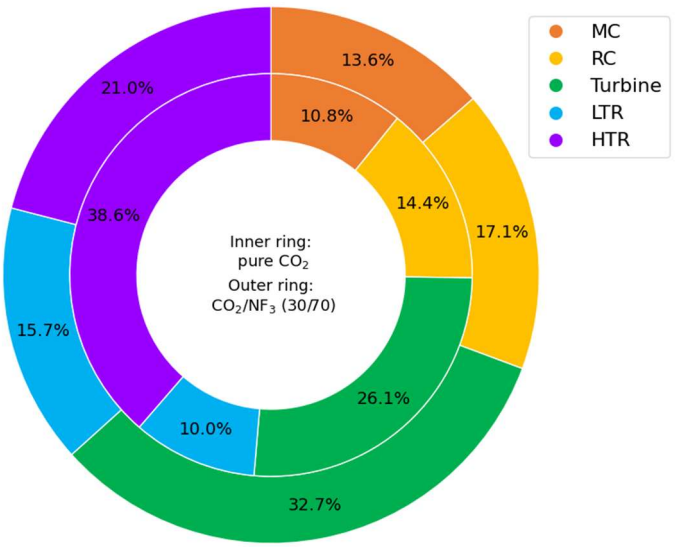

(a)

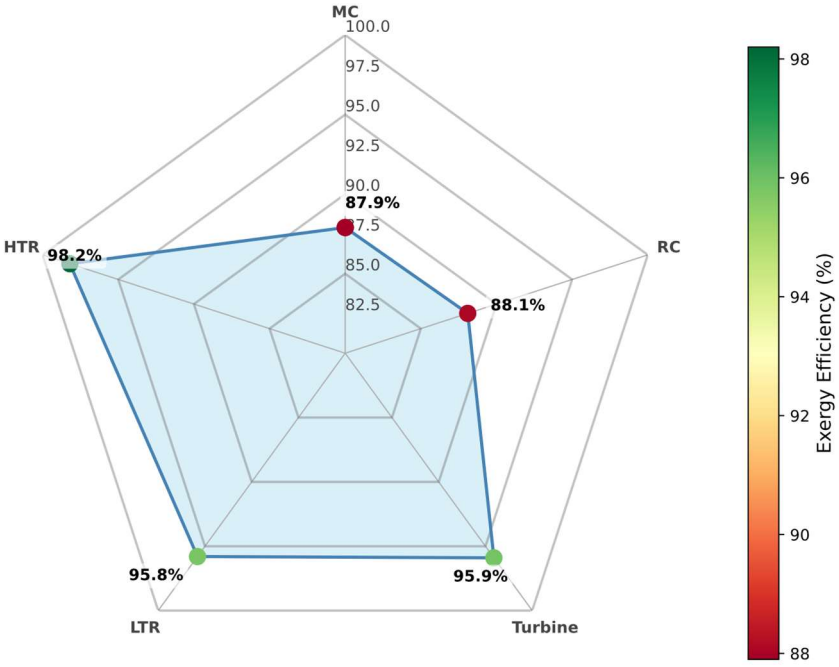

(b)

Figure 15. (a) Exergy destruction and (b) Exergy efficiency with CO_2/NF_3 mixture.

3.6.5 CO_2/Kr Mixture

The krypton mixture aligns with the observed trend of the other mixtures that have been examined. The analysis demonstrates a significant reduction in exergy destruction across all components, apart from the HTR. However, the exergy efficiency is marginally higher in the MC and HTR.

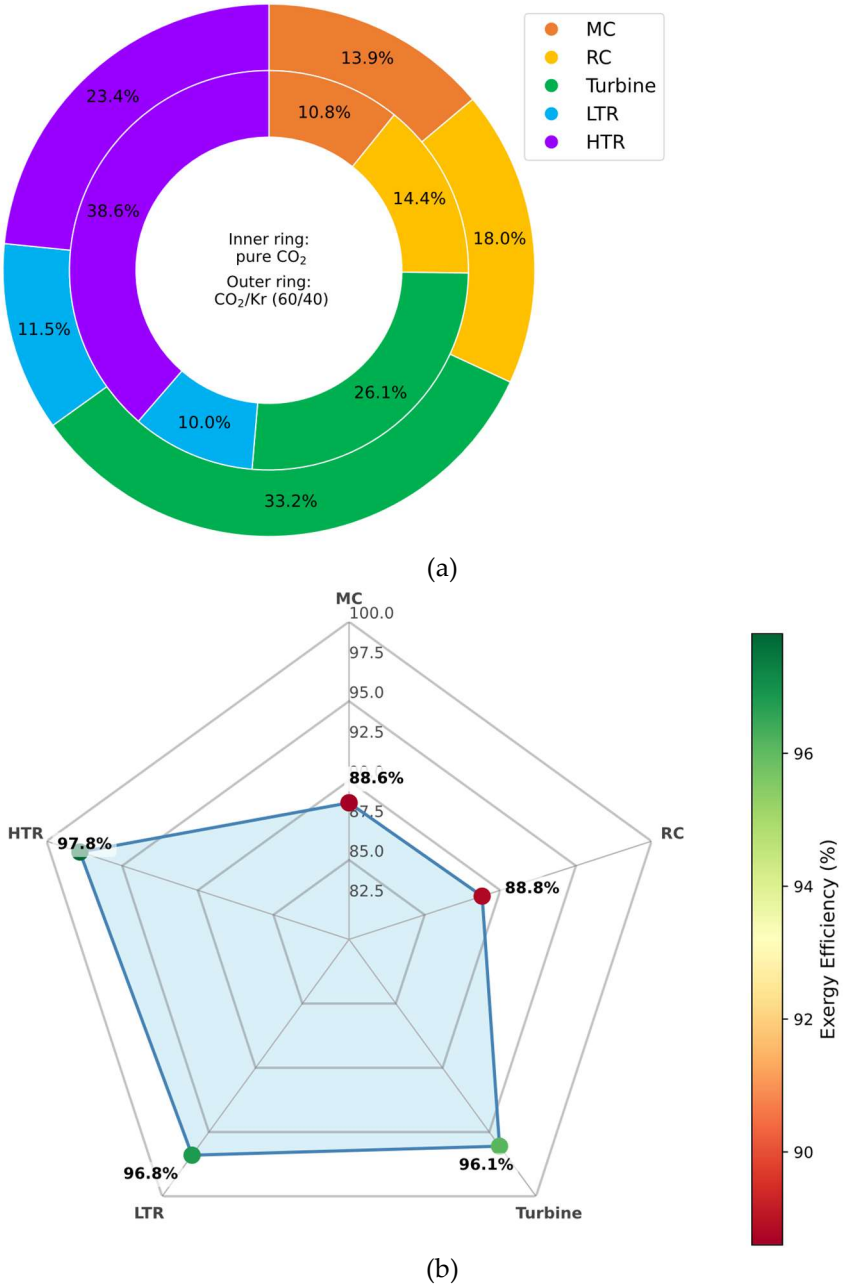

Figure 16. (a) Exergy destruction and (b) Exergy efficiency with CO_2/Kr mixture.

As illustrated in Table 4, according to equation 33, a comparative analysis of the results pertaining to the cycle's thermal efficiency, equivalent Carnot efficiency, the composition of irreversibilities, and the total entropy generation for the diverse range of fluids examined in this study is presented.

Table 4. Summary of the results obtained for the RBC.

Working Fluid	η_{th}	$\eta_{Eq-Carnot}$	$\sigma_{total}\left(\frac{kW}{K}\right)$
Pure CO_2	0.4568	0.6322	12.39
CO_2/CF_4 (21/79)	0.5770	0.7228	10.15
CO_2/CH_4 (10/90)	0.5859	0.7389	11.77
CO_2/NF_3 (30/70)	0.5350	0.6992	11.38
CO_2/Kr (60/40)	0.5125	0.6637	10.77

4. Conclusions

In summary, blending CO_2 with select low-critical-temperature gases markedly enhances the thermodynamic performance of s-CO_2 Brayton power cycles in cold ambient conditions. The binary mixtures examined (CO_2 with CF_4, CH_4, NF_3, and Kr) demonstrated significant improvements over pure CO_2, including higher cycle efficiencies, lower specific compressor work, larger turbine expansion ratios, and more effective recuperation at the cold end of the cycle. By lowering the working fluid's critical point, these blends avoid two-phase instabilities near the compressor inlet and allow the turbine to expand the fluid further without condensation, directly increasing work output and reducing compression power input. Consequently, net efficiency gains on the order of several percentage points were achieved. Notably, at ambient temperatures of –40 °C to –50 °C, the CO_2/NF_3, CO_2/CF_4, and CO_2/CH_4 mixtures yielded approximately a 10% increase in thermal efficiency compared to the pure s-CO_2 cycle. This substantial improvement is consistent with prior observations that the farther the ambient conditions deviate below CO_2's normal operating range, the greater the benefit of an optimized working fluid blend.

The performance gains depended strongly on the mixture of composition and heat exchanger characteristics. In general, increasing the fraction of the additive (thus lowering the mixture critical temperature) led to better cold-weather performance. Each binary pair exhibited an optimal composition range where efficiency was maximized. High additive concentrations (50–90% by molar fraction) were most effective for maintaining supercritical operation at very low temperatures, as they significantly depress the critical point and diminish CO_2's tendency to liquefy. For example, using a blend of 20% CO_2 / 80% Kr enabled a peak cycle efficiency of about 52.5%, a noticeable improvement over the pure CO_2 baseline. However, Krypton's mixture provided somewhat smaller relative gains than the other additives, and its practical use may be limited by cost and scarcity. In contrast, NF_3, CF_4, and CH_4 mixtures delivered robust efficiency improvements (on the order of 7–10%) within the 50–80% additive range, making them attractive for cold-climate applications. These blends effectively mitigate the compressor inlet condensation issue by "floating" the cycle's critical point to lower temperatures, which stabilizes the fluid state and reduces compressor work for a given pressure ratio. Additionally, the mixtures exhibited more favorable heat-transfer characteristics in the recuperators; the altered thermophysical properties (heat capacity profiles and higher hot-to-cold temperature differentials) enabled greater recuperation of turbine exhaust heat at the low temperature end of the cycle.

Importantly, the extent of the efficiency gain was found to depend on the heat exchanger conductance (UA) available in the recuperation system. If the recuperators are not sized adequately, a portion of the potential heat recovery benefit from the mixtures cannot be realized due to pinch-point limitations. Our simulation results showed that increasing the total UA of the recuperators boosts cycle efficiency, allowing the working-fluid blends to reach their full performance potential. Cycle's efficiency improvement climbed as recuperator UA was raised. This trend underlines that the improved thermal recuperation capacity of the mixtures must be matched by appropriate exchanger sizing. In practical terms, the high-temperature recuperator (HTR) should be resized (enlarged) to handle the higher heat duty generated when using these high-additive mixtures, ensuring that the additional low-grade heat is captured rather than wasted. This design adjustment is essential to fully capitalize on the mixtures' enhanced recuperative behavior and to avoid bottlenecking the efficiency gains.

Based on the above findings, we recommend employing binary CO_2-based mixtures with roughly 50–90% additive content (by mole) when designing s-CO_2 Brayton power systems for sub-zero ambient environments. Working fluids in this composition range provide a good balance of thermodynamic performance and operational stability, keeping the compressor inlet well above the saturation line even in environments far below 0 °C.

Such mixtures (for example, $CO_2/CF_4 \approx 30/70$ or $CO_2/NF_3 \approx 20/80$) enable the cycle to maintain single-phase supercritical conditions throughout, thereby minimizing compressor work and maximizing turbine expansion in cold climates.

Furthermore, this work advises an increasing the size (UA value) of the high-temperature recuperator to accommodate the greater heat-recovery duty of these mixtures. Enlarging the HTR (or adding additional recuperation capacity) allows the cycle to exploit the mixtures' improved heat recovery potential, yielding higher overall efficiency. In summary, a combination of high-additive working-fluid blends and appropriately scaled recuperators can achieve substantially better efficiency and more reliable operation for s-CO_2 Brayton power plants in cold regions, as compared to the conventional pure-CO_2 cycle. These modifications help ensure that the cycle maintains high efficiency across a wider range of ambient temperatures than would be possible with CO_2 alone.

The exergy efficiency of the different cycle components when using mixtures remains similar in most cases. However, in the high-temperature heat recovery (HTR), a higher exergy efficiency is achieved when using the CO_2/CF_4 mixture, with a value of 99.1%. It should be noted that the HTR is the component with the highest exergy efficiency in the cycle, regardless of whether pure CO_2 or binary mixtures are used.

Design Recommendations

Based on the insights gained from this work, several actionable recommendations can be made for the design of high efficiency s-CO_2 Brayton cycles for cold climate applications:

Working Fluid Selection

Binary CO_2-based mixtures containing 50–90% molar concentration of low-critical-temperature additives (CF_4, CH_4, NF_3) are recommended for systems intended to operate in sub-zero ambient environments. These mixtures ensure stable supercritical operation, minimize compressor work, and maximize turbine expansion ratios even at ambient temperatures as low as –50 °C.

Heat Exchanger Design Optimization

The low-temperature recuperator should be resized—potentially significantly enlarged—to accommodate the increased heat recovery duty associated with these mixtures. System designers should target HTR UA values exceeding 5,000 kW/K for CH_4- and CF_4-rich blends to prevent pinch-point constraints and fully capitalize on the improved recuperative performance.

System-Level Integration Considerations

While CH_4-based mixtures offer the highest theoretical cycle efficiencies, their substantial volumetric flow penalties and turbomachinery scaling challenges necessitate careful techno-economic assessments. Conversely, CF_4 and NF_3 mixtures offer more favorable integration profiles and may present the most practical pathway for retrofitting or upgrading existing s-CO_2 systems to cold-climate operation.

Environmental and Economic Considerations

Given the high global warming potential (GWP) and potential environmental implications of fluorinated additives such as CF_4 and NF_3, future designs should explore mixtures that balance performance with environmental sustainability, considering lifecycle emissions, leakage mitigation strategies, and potential alternative additives with lower GWP profiles.

Future work

Looking ahead, the promising results with binary mixtures suggest that ternary mixtures (CO_2 plus two additives) could unlock even greater performance benefits. In particular, blends that include an ideal or near-ideal gas component (such as Argon, Xenon, carbon monoxide, or nitrogen) alongside CO_2 and a second condensing species merit

investigation. Preliminary analyses indicate that carefully chosen ternary combinations can further tailor the fluid properties to extreme cold conditions (below –50 °C), offering even higher efficiencies and enhanced stability in simulations. For example, adding inert gases like Ar or N_2 can reduce the reliance on high-GWP fluorinated additives by lowering the mixture critical point through dilution while improving specific heat ratios, which yields environmental and cost advantages without sacrificing performance. Likewise, a heavier but relatively inert gas such as Xe or a diatomic like CO can be introduced to finetune the working fluid's molecular complexity and heat capacity. These three-component blends leverage the complementary benefits of each constituent – the heavy molecules provide increased density and recuperation capability; the lighter ideal gases improve fluid stability and reduce greenhouse impact – resulting in superior cold-weather thermodynamic behavior. In fact, certain ternary mixtures in our exploratory simulations not only match but exceed the efficiency gains of the best binary cases, all while using more benign components. This points to a strong pathway for sustainable, high efficiency s-CO_2 power systems in ultra-cold climates. Future research should focus on optimizing these ternary formulations, experimentally validating their thermophysical performance, and assessing long-term operability (materials compatibility, leakage, etc.) to pave the way for next-generation cold-climate Brayton cycle power plants.

Author Contributions: Conceptualization, P.T.-E. and L.C.-E.; methodology, L.C.-E.; software, L.C.-E.; validation, R.V.-C., J.M.-A. and P.T.-E; formal analysis, L.C.-E.; investigation, L.C.-E..; resources, L.C.-E.; data curation, R.V.-C.; writing—original draft preparation, L.C.-E. and P.T.-E.; writing—review and editing, R.V.-C. and J.M.-A.; visualization, L.C.-E.; supervision, J.M.-A. All authors have read and agreed to the published version of the manuscript.

Funding: This research received no external funding.

Institutional Review Board Statement: Not applicable.

Data Availability Statement: Data will be made available on request.

Acknowledgments: The authors would like to express their gratitude to the Thermal Energy for Sustainability (TE4S) Research Group of the Universidad Politécnica de Madrid for their invaluable support. In addition, the authors wish to extend their profound thanks to the FOCAPRO and GICFOR groups of the Universidad Técnica del Norte for their indispensable contribution to this research.

Conflicts of Interest: The authors declare no conflicts of interest.

Nomenclature

Abbreviations

CF_4	Tetrafluoromethane
CH_4	Methane
CIP	Compressor inlet pressure
CIT	Compressor inlet temperature
CO_2	Carbon dioxide
CSP	Concentrated solar power
LT	Low temperature
h	Specific enthalpy [kJ/kg]
HT	High temperature
HTR	High temperature recuperator
Kr	Krypton
NF_3	Nitrogen Trifluoride

MC	Main Compressor
$\dot{m}_{comp}$	Mass flow of the compressor [kg/s]
$\dot{m}_{turb}$	Mass flow of the turbine [kg/s]
NIST	National Institute of Standards and Technology
RBC	Recompression Brayton cycle
RC	Recompressor
LTR	Low temperature recuperator
PC	Pre-Compressor
PHX	Primary heat exchanger
$P_{MC,out}$	Compressor outlet pressure
PreC	Precooler
$\dot{Q}$	Heat transfer ratio
s	Specific entropy [kJ/kg·K]
s-CO_2	Supercritical carbon dioxide
SCSP	Supercritical concentrated solar power plant
T_0	Ambient temperature [K]
T_{abs}	Absorption temperature [K]
T_{rej}	Rejection temperature [K]
UA_{total}	Heat total recuperator conductance [kW/K]
$\dot{W}$	Power [kW]

Greek Symbols

$\eta_{Eq-Carnot}$	Equivalent Carnot efficiency
η_{comp}	Compressor efficiency
η_g	Generator efficiency
η_{turb}	Turbine efficiency
η_{th}	Thermal efficiency
η_{ex}	Exergy efficiency
$\dot{\sigma}$	Entropy generated [kW/K]
γ	Split flow ratio

References

1. M.T. White, G. Bianchi, L. Chai, S.A. Tassou, A.I. Sayma, Review of supercritical CO_2 technologies and systems for power generation, Appl. Therm. Eng. 185 (2021) 116447. https://doi.org/10.1016/j.applthermaleng.2020.116447
2. Y. Liang, X. Lin, W. Su, L. Xing, N. Zhou, Thermal-economic analysis of a novel solar power tower system with CO_2-based mixtures at typical days of four seasons, Energy 276 (2023) 127602. https://doi.org/10.1016/j.energy.2023.127602
3. F. Crespi, P. Rodríguez de Arriba, D. Sánchez, A. Muñoz, Preliminary investigation on the adoption of CO_2–SO_2 working mixtures in a transcritical Recompression cycle, Appl. Therm. Eng. 211 (2022) 118384. https://doi.org/10.1016/j.applthermaleng.2022.118384
4. S. Jeong, S.Y. Kim, Y. Lee, J. Lee, J. Jeong, CO_2-based binary mixtures for sodium-cooled fast reactor power systems, Ann. Nucl. Energy 45 (2012) 10–20. https://doi.org/10.1016/j.anucene.2012.01.011
5. S.Y. Kim, S. Jeong, Performance comparison of recompression supercritical CO_2 cycles with different working fluids for sodium-cooled fast reactors, Nucl. Eng. Technol. 45 (2013) 565–574. https://doi.org/10.5516/NET.03.2012.032
6. S. Jeong, Y. Lee, J. Lee, J. Jeong, Application of CO_2-based mixtures to increase thermal efficiency in nuclear power systems, Energy 49 (2013) 187–197. https://doi.org/10.1016/j.energy.2012.11.013
7. D. Bonalumi, A. Casati, G. Lozza, Thermodynamic optimization of CO_2/$TiCl_4$ supercritical cycle, Appl. Energy 113 (2014) 1225–1235. https://doi.org/10.1016/j.apenergy.2013.08.053
8. C.M. Invernizzi, E. Martelli, Experimental study of $TiCl_4$–CO_2 mixtures for power cycle applications, Energy Procedia 101 (2016) 1251–1258. https://doi.org/10.1016/j.egypro.2016.11.167
9. G. Di Marcoberardino, E. Morosini, G. Manzolini, Experimental and analytical procedure for the characterization of innovative working fluids for power plants applications, Appl. Therm. Eng. 178 (2020) 115513. https://doi.org/10.1016/j.applthermaleng.2020.115513

10. O.A. Aqel, M.T. White, M.A. Khader, A.I. Sayma, Sensitivity of transcritical cycle and turbine design to dopant fraction in CO_2-based working fluids, Appl. Therm. Eng. 190 (2021) 116796. https://doi.org/10.1016/j.applthermaleng.2021.116796
11. R. Valencia-Chapi, L. Coco-Enríquez, J. Muñoz-Antón, Supercritical CO_2 mixtures for advanced Brayton power cycles in line-focusing solar power plants, Appl. Sci. 10 (2020) 55. https://doi.org/10.3390/app10010055
12. F. Crespi, P. Rodríguez-de-Arriba, D. Sánchez, A. Muñoz, A methodology to design air-cooled condensers for supercritical power cycles using carbon dioxide and carbon dioxide mixtures, European sCO_2 Conference (2024). https://doi.org/10.17185/duepublico/77329
13. L. Wang, L.-m. Pan, J. Wang, D. Chen, Y. Huang, W. Sun, L. Hu, Investigation on the effect of mixtures physical properties on cycle efficiency in the CO_2-based binary mixtures Brayton cycle, Prog. Nucl. Energy 143 (2022) 104049. https://doi.org/10.1016/j.pnucene.2021.104049
14. V.C. Illyés, G. Di Marcoberardino, A. Werner, M. Haider, G. Manzolini, Experimental evaluation of the CO_2-based mixture CO_2/C_6F_6 in a recuperated transcritical cycle, Energy 313 (2024) 133713. https://doi.org/10.1016/j.energy.2024.133713
15. P.M. Tafur-Escanta, R. Valencia-Chapi, J. Muñoz-Antón, Exergetic and Entropy Analysis of the PCRC and RCMCI Brayton Cycles Using s-CO_2 Mixtures. Case Study: Marine Applications, European sCO_2 Conference (2024). https://doi.org/10.17185/duepublico/77263
16. M. Doninelli, E. Morosini, D. Alfani, M. Astolfi, G. Di Marcoberardino, G. Manzolini, Analysis of the potential of CO_2 based mixtures to improve the efficiency of cogenerative waste heat recovery power plants, European sCO_2 Conference (2024). https://doi.org/10.17185/duepublico/77287
17. P. Rodríguez-de-Arriba, F. Crespi, S. Pace, D. Sánchez, Mapping the techno-economic potential of next-generation CSP plants running on transcritical CO_2-based power cycles, Energy 310 (2024) 133142. https://doi.org/10.1016/j.energy.2024.133142
18. L. Vesely, K.R.V. Manikantachari, S. Vasu, J. Kapat, V. Dostal, S. Martin, Effect of impurities on compressor and cooler in supercritical CO_2 cycles, J. Energy Resour. Technol. 141 (2019) 012003. https://doi.org/10.1115/1.4040581
19. X. Wang, L. Zhang, Z. Zhu, M. Hu, J. Wang, X. Fan, Performance improvement overview of the supercritical carbon dioxide Brayton cycle, Processes 11 (2023) 2795. https://doi.org/10.3390/pr11092795
20. A.S. Abdeldanyem, M.T. White, A. Paggini, M. Ruggiero, A.I. Sayma, Integrated aerodynamic and structural blade shape optimization of axial turbines operating with supercritical carbon dioxide blended with dopants, J. Eng. Gas Turbines Power 144 (2022) 101016. https://doi.org/10.1115/1.4055232
21. S.I. Salah, F. Crespi, M.T. White, A. Muñoz, A. Paggini, M. Ruggiero, D. Sánchez, A.I. Sayma, Axial turbine flow path design for concentrated solar power plants operating with CO_2 blends, Appl. Therm. Eng. 230 (2023) 120612. https://doi.org/10.1016/j.applthermaleng.2023.120612
22. A.S. Abdeldanyem, S.I. Salah, M.T. White, A.I. Sayma, A modified loss breakdown approach for axial turbines operating with blended supercritical carbon dioxide, J. Eng. Gas Turbines Power 145 (2023) 081002. https://doi.org/10.1115/1.4062478
23. Liu, J.; Yu, A.; Lin, X.; Su, W.; Ou, S. Performances of Transcritical Power Cycles with CO_2-Based Mixtures for the Waste Heat Recovery of ICE. Entropy 2021, 23, 1551. https://doi.org/10.3390/e23111551
24. A. Yu, W. Su, L. Zhao, X. Lin, N. Zhou, New knowledge on the performance of supercritical Brayton cycle with CO_2-based mixtures, Energies 13 (2020) 1741. https://doi.org/10.3390/en13071741
25. E. Morosini, D. Alfani, S.I. Salah, A. Abdeldanyem, F. Crespi, G. Di Marcoberardino, G. Manzolini, Off-design of a CO_2-based mixture transcritical cycle for CSP applications: Analysis at part load and variable ambient temperature, Appl. Therm. Eng. 236 (2024) 121735. https://doi.org/10.1016/j.applthermaleng.2023.121735
26. M. Doninelli, G. Di Marcoberardino, C.M. Invernizzi, P. Iora, Experimental isochoric apparatus for bubble points determination: Application to CO_2 binary mixtures as advanced working fluids, Int. J. Thermofluid. 23 (2024) 100742. https://doi.org/10.1016/j.ijft.2024.100742
27. M. Baiguini, M. Doninelli, E. Morosini, D. Alfani, G. Di Marcoberardino, P.G. Iora, G. Manzolini, C.M. Invernizzi, M. Astolfi, Small scale CO_2 based trigeneration plants in heat recovery applications, Appl. Therm. Eng. 255 (2024) 123943. https://doi.org/10.1016/j.applthermaleng.2024.123943
28. M. Baiguini, G. Di Marcoberardino, P.G. Iora, High-temperature electrolysis integrated with advanced power cycles for the combined production of green hydrogen, heat and power, Energy Convers. Manag. 322 (2024) 119121. https://doi.org/10.1016/j.enconman.2024.119121
29. Y.-N. Ma, P. Hu, Thermo-economic comparative study and multi-objective optimization of supercritical CO_2-based mixtures Brayton cycle combined with absorption refrigeration cycle, J. Therm. Sci. Eng. Appl. 15 (2023) 084501. https://doi.org/10.1115/1.4062435

30. NIST Chemistry WebBook, Critical Properties of Krypton, Methane, CF_4, NF_3. https://webbook.nist.gov/chemistry
31. IPCC Fifth Assessment Report (AR5) – Global Warming Potentials. https://www.ipcc.ch/report/ar5/
32. M. Doninelli, E. Morosini, G. Di Marcoberardino, C.M. Invernizzi, P. Iora, Experimental characterization of CO_2–$SiCl_4$ mixture as innovative working fluid, Energy 299 (2024) 131197. https://doi.org/10.1016/j.energy.2024.131197
33. F. Crespi, P. Rodríguez-de-Arriba, D. Sánchez, L. García-Rodríguez, Principles of operational optimization of CSP plants based on carbon dioxide mixtures, Appl. Therm. Eng. 260 (2025) 124871. https://doi.org/10.1016/j.applthermaleng.2024.124871
34. Q. Deng, A. Liu, J. Li, Z. Feng, A review on supercritical CO_2 and CO_2-based mixture in power cycle, Energy Convers. Manag. 324 (2025) 119295. https://doi.org/10.1016/j.enconman.2024.119295
35. Dyreby, J.J. Modeling the Supercritical Carbon Dioxide Brayton Cycle with Recompression. Ph.D. Thesis, University of Wisconsin–Madison, 2014. https://sel.me.wisc.edu/publications/theses/dyreby14.zip
36. Coco-Enríquez, L. Nueva Generación de Centrales Termosolares con Colectores Solares Lineales Acoplados a Ciclos Supercríticos de Potencia. Ph.D. Thesis, UPM, Spain, 2017. http://dx.doi.org/10.20868/UPM.thesis.44002
37. Y. Çengel, M. Boles, and M. Kanoglu, Thermodynamics. An Engineering Approach, 10th ed. McGraw Hill, 2024. Accessed: Feb. 10, 2025. [Online]. Available: https://www.mheducation.com/highered/product/thermodynamics-an-engineering-approach-cengel.html
38. K. Ökten and B. Kurşun, "Thermo-economic assessment of a thermally integrated pumped thermal energy storage (TI-PTES) system combined with an absorption refrigeration cycle driven by low-grade heat source," J Energy Storage, vol. 51, Jul. 2022, https://doi.org/10.1016/j.est.2022.104486
39. O. P. Sharma, S. C. Kaushik, and K. Manjunath, "Thermodynamic analysis and optimization of a supercritical CO2 regenerative recompression Brayton cycle coupled with a marine gas turbine for shipboard waste heat recovery," Thermal Science and Engineering Progress, vol. 3, pp. 62–74, Sep. 2017, https://doi.org/10.1016/j.tsep.2017.06.004
40. R. Nieto-Carlier, C. Gonzalez-Fernandez, I. Lopez-Paniagua, A. Jimenez-Alvaro, and J. Rodriguez-Marin, Termodinámica. Dextra Editorial S.L., 2014, https://l1nq.com/kBQVo
41. D. E. Winterbone and Ali. Turan, Advanced Thermodynamics for Engineers, Second. Elsevier Ltd, 2015, https://doi.org/10.1016/C2013-0-13437-X
42. P. Tafur-Escanta, I. López-Paniagua, and J. Muñoz-Antón, "Thermodynamics Analysis of the Supercritical CO2 Binary Mixtures for Brayton Power Cycles," Energy, vol. 270, May 2023, https://doi.org/10.1016/j.energy.2023.126838
43. Lemmon, E.W. et al., NIST Standard Reference Database 23: REFPROP Version 10.0 (2018). https://www.nist.gov/srd/refprop
44. Follett IV, W. W., Moore, J., Wade, J., & Pierre, S. (2024). The STEP 10 MWe sCO_2 pilot installation and commissioning status update. Proceedings of the 8th International Supercritical CO_2 Power Cycles Symposium (Paper #74), February 26–29, 2024, San Antonio, TX, USA. https://sco2symposium.com/proceedings2024/74-paper.pdf
45. P. Tafur-Escanta, R. Valencia-Chapi, J. Rodríguez-Martín, and J. Muñoz-Antón, "Brayton Cycle Using s-CO2 Mixtures as Working Fluid for Pumped Thermal Energy Storage: Exergy and Cost Analysis," 6th Edition of the European Conference on Supercritical CO2 (sCO2) for Energy Systems: April 09–11, 2025, Delft, The Netherlands. in Conference Proceedings of the European sCO2 Conference. pp. 88–98, Apr. 28, 2025, https://duepublico2.uni-due.de/receive/duepublico_mods_00083284
46. Tafur-Escanta, P., Valencia-Chapi, R., & Muñoz-Antón, J. (2025). Entropy analysis of new proposed Brayton cycle configurations for solar thermal power plants. Thermal Science and Engineering Progress, 62, 103670. https://doi.org/10.1016/j.tsep.2025.103670